Applied Mathematical Modelling 84 (2020) 324–356

Contents lists available at ScienceDirect

Applied Mathematical Modelling

journal homepage: www.elsevier.com/locate/apm

Practical uncertainty quantification analysis involving statistically dependent random variables☆

Dongjin Lee, Sharif Rahman*

College of Engineering, The University of Iowa, Iowa City, Iowa 52242, USA

ARTICLE INFO

Article history:
Received 9 October 2019
Revised 5 March 2020
Accepted 26 March 2020
Available online 9 April 2020

Keywords:
Generalized polynomial chaos expansion
D-MORPH regression
Multivariate orthonormal polynomials
Monomial moment matrix
Second-moment analysis
Reliability analysis

ABSTRACT

This article presents a practical refinement of generalized polynomial chaos expansion for uncertainty quantification under dependent input random variables. Unlike the Rodrigues-type formula, which exists for select probability measures, a three-step computational algorithm is put forward to generate a sequence of any approximate measure-consistent multivariate orthonormal polynomials. For uncertainty quantification analysis under dependent random variables, two regression methods, comprising existing standard least-squares and newly developed partitioned diffeomorphic modulation under observable response preserving homotopy (D-MORPH), are proposed to estimate the coefficients of generalized polynomial chaos expansion for the very first time. In contrast to the existing regression devoted so far to the classical polynomial chaos expansion, no tensor-product structure is required or enforced. The partitioned D-MORPH regression is applicable to either an underdetermined or overdetermined system, thus substantially enhancing the ability of the original D-MORPH regression. Numerical results obtained for Gaussian and non-Gaussian probability measures with rectangular or non-rectangular domains point to highly accurate orthonormal polynomials produced by the three-step algorithm. More significantly, the generalized polynomial chaos approximations of mathematical functions and stochastic responses from solid-mechanics problems, in tandem with the partitioned D-MORPH regression, provide excellent estimates of the second-moment properties and reliability from only hundreds of function evaluations or finite element analyses.

1. Introduction

Uncertainty quantification (UQ) is an important scientific driver for mathematical modeling, simulation, and design of complex mechanical systems. Modern methods for UQ analysis, often viewed as surrogates for expensive-to-run computational models, are polynomial chaos expansion (PCE) [1,2], polynomial dimensional decomposition (PDD) [3,4], stochastic collocation [5,6], and sparse-grid quadrature [7,8], to name a few. All of these methods, including a few not explicitly mentioned here for brevity, are known to achieve substantial computational advantages over standard Monte Carlo simulation (MCS). However, most, if not all, existing methods are grounded on the independence supposition of input random variables. In a practical setting, though, significant correlation or dependence prevails among input variables, undermining or negating the applicability of most methods available today. Dismissing this correlation or dependence, whether stemming from loads,

☆ Grant sponsor: U.S. National Science Foundation; Grant No. CMMI-1607398.
* Corresponding author.
E-mail addresses: dongjin-lee@uiowa.edu (D. Lee), rahman@engineering.uiowa.edu, sharif-rahman@uiowa.edu (S. Rahman).

https://doi.org/10.1016/j.apm.2020.03.041
0307-904X/

geometry, or material properties, is usually not recommended, as it may produce inaccurate prediction of the probabilistic response characteristics, leading to an unsatisfactory design [9]. A mapping method, such as the Rosenblatt transformation [10], is commonly employed to transform dependent to independent input variables, thereby enabling the usage of classical PCE for dependent input. However, it creates very high nonlinearity to input–output relation of a stochastic system, degrading convergence of the probabilistic solution [11]. Therefore, new methods or suitably enhanced existing methods must be generated for UQ analysis in the presence of random input bequeathed with arbitrary dependent probability distributions.

A handful of UQ methods accounting for statistical correlation or dependence in random input have already appeared [12–14]. These methods, essentially the generalizations of PCE [12] and PDD [13,14], entail Fourier or Fourier-like series expansions comprising measure-consistent multivariate orthonormal polynomials in dependent variables. By tackling dependent random variables straight on, they circumvent a potentially detrimental measure transformation between dependent and independent variables [11], thereby establishing a step in the right direction towards general UQ analysis. But, still, these methods suffer from two important limitations, impeding their full potential. First, multivariate orthonormal polynomials consistent with the input probability measure must be generated. Although they are easily produced for classical probability density functions endowed with a Rodrigues-type formula [13,15], creating such polynomials for realistic probability measures in a practical setting is unlikely, if not impossible. Instead, numerical approximations must be used. In this regard, the well-known Gram-Schmidt process can be employed to generate from monomials a sequence of orthonormal polynomials. In the work by Navarro et al. [16], this method was employed for solving two- or three- dimensional stochastic problems. However, due to ill-conditioning, the Gram-Schmidt method is restricted to low-dimensional problems with low-order approximations. Thus, more stable methods are needed to compute high-order orthogonal polynomials in high dimensions. Second, the calculation of the expansion coefficients of the generalized PCE or PDD requires evaluating a myriad of high-dimensional integrals. They cannot be determined analytically or exactly if the response function is a general one or the input probability measure is arbitrary. Furthermore, a full numerical integration employing tensor product of a univariate quadrature formula is computationally expensive and likely prohibitive. Therefore, alternative means of estimating these integrals must be pursued. Only by resolving these two limitations will the aforementioned generalized versions be able to reach their ultimate potential in solving practical UQ problems subject to truly arbitrary distributions of random input. The development of such capabilities is the chief motivation for this work.

The core objective of this study is to create a constructive version of the generalized PCE (GPCE) for UQ analysis of uncertain mechanical systems in the presence of arbitrary, dependent probability measures of input variables. While this paper addresses the practical aspect of GPCE, readers interested in the mathematical foundation of GPCE should check the prequel [12]. The paper is structured as follows. Section 2 discusses mathematical notations and preliminaries, including a list of requisite assumptions. A brief exposition of measure-consistent multivariate orthonormal polynomials, including a practical means for their construction, is given in Section 3. Section 4 summarizes GPCE and its truncated version, resulting in the concomitant formulae and equations for estimating the second-moment properties and reliability associated with a general response variable of interest. Section 5 outlines a procedure for generating approximate measure-consistent orthonormal polynomials in a practical setting. In Section 6, two regression methods are presented to estimate the GPCE coefficients. An algorithm for practical implementation of the GPCE method is also outlined in Section 7. Numerical results generated from three example problems are reported in Section 8. Section 9 discusses the future outlook. Finally, the conclusions are drawn in Section 10.

2. A general UQ problem under dependent variables

Let $\mathbb{N} := \{1, 2, \ldots\}$, $\mathbb{N}_0 := \mathbb{N} \cup \{0\}$, $\mathbb{R} := (-\infty, +\infty)$, and $\mathbb{R}_0^+ := [0, +\infty)$ represent the sets of positive integer (natural), non-negative integer, real, and non-negative real numbers, respectively. For a finite integer $N \in \mathbb{N}$, denote by $\mathbb{A}^N \subseteq \mathbb{R}^N$ a bounded or unbounded subdomain of $\mathbb{R}^N$. The set of $N \times N$ real-valued square matrices is denoted by $\mathbb{R}^{N\times N}$.

2.1. Input random variables

Let $(\Omega, \mathcal{F}, \mathbb{P})$ be a complete probability triple, where Ω is a sample space representing an abstract set of elementary events, $\mathcal{F}$ is a σ-algebra on Ω, and $\mathbb{P} : \mathcal{F} \to [0, 1]$ is a probability measure. With $\mathcal{B}^N := \mathcal{B}(\mathbb{A}^N)$ representing the Borel σ-algebra on $\mathbb{A}^N \subseteq \mathbb{R}^N$, consider an $\mathbb{A}^N$-valued random vector $\mathbf{X} := (X_1, \ldots, X_N)^\intercal : (\Omega, \mathcal{F}) \to (\mathbb{A}^N, \mathcal{B}^N)$, describing the statistical uncertainties in all input and system parameters of a stochastic or UQ problem. Every so often, $\mathbf{X}$ will be referred to as an input random vector or variables and the integer N, representing the total number of input random variables, will be designated as the dimension of the UQ problem. As an example, consider a simply supported beam with random length L, random moment of inertia I, and random Young's modulus E, which is subjected to two vertically applied concentrated forces F_1 and F_2. If all of these input parameters are modeled as random variables, then the UQ problem involves an input random vector $\mathbf{X} := (L, I, E, F_1, F_2)^\intercal$ with dimension $N = 5$.

Denote by $F_{\mathbf{X}}(\mathbf{x}) := \mathbb{P}\big[\cap_{i=1}^N \{X_i \le x_i\}\big]$ the joint distribution function of $\mathbf{X}$, admitting the joint probability density function $f_{\mathbf{X}}(\mathbf{x}) := \partial^N F_{\mathbf{X}}(\mathbf{x})/\partial x_1 \cdots \partial x_N$. Given the abstract probability space $(\Omega, \mathcal{F}, \mathbb{P})$, the image probability space is $(\mathbb{A}^N, \mathcal{B}^N, f_{\mathbf{X}} d\mathbf{x})$, where $\mathbb{A}^N$ can be viewed as the image of Ω from the mapping $\mathbf{X} : \Omega \to \mathbb{A}^N$, and is also the support of $f_{\mathbf{X}}(\mathbf{x})$.

A set of requisite assumptions for UQ analysis conducted is as follows.

Assumption 1. The random vector $\mathbf{X} := (X_1, \ldots, X_N)^\intercal : (\Omega, \mathcal{F}) \to (\mathbb{A}^N, \mathcal{B}^N)$

(1) has an absolutely continuous joint distribution function $F_{\mathbf{X}}(\mathbf{x})$ and a continuous joint probability density function $f_{\mathbf{X}}(\mathbf{x})$ with a bounded or unbounded support $\mathbb{A}^N \subseteq \mathbb{R}^N$;
(2) possesses absolute finite moments of all orders, that is, for all $\mathbf{j} := (j_1, \ldots, j_N) \in \mathbb{N}_0^N$,

$$\mathbb{E}\left[|\mathbf{X}^{\mathbf{j}}|\right] := \int_\Omega |\mathbf{X}(\omega)|^{\mathbf{j}} d\mathbb{P}(\omega) = \int_{\mathbb{A}^N} |\mathbf{x}^{\mathbf{j}}| f_{\mathbf{X}}(\mathbf{x}) d\mathbf{x} < \infty,$$

where $\mathbf{X}^{\mathbf{j}} = X_1^{j_1} \cdots X_N^{j_N}$ and $\mathbb{E}$ is the expectation operator with respect to the probability measure $\mathbb{P}$ or $f_{\mathbf{X}}(\mathbf{x})d\mathbf{x}$; and
(3) has a joint probability density function $f_{\mathbf{X}}(\mathbf{x})$, which
  (a) has a compact support, that is, there exists a compact subset $\mathbb{A}^N \subset \mathbb{R}^N$ such that $\mathbb{P}[\mathbf{X} \in \mathbb{A}^N] = 1$, or
  (b) is exponentially integrable, that is, there exists a real number $\alpha > 0$ such that

$$\int_{\mathbb{A}^N} \exp(\alpha \|\mathbf{x}\|) f_{\mathbf{X}}(\mathbf{x}) d\mathbf{x} < \infty,$$

where $\|\cdot\| : \mathbb{A}^N \to \mathbb{R}_0^+$ is an arbitrary norm.

Assumption 1 is identical to what is reported in the previous paper [12]. Readers are directed to prior work for further explanation.

2.2. Output random variable

Given an input random vector $\mathbf{X} := (X_1, \ldots, X_N)^\intercal : (\Omega, \mathcal{F}) \to (\mathbb{A}^N, \mathcal{B}^N)$ with known probability density function $f_{\mathbf{X}}(\mathbf{x})$ on $\mathbb{A}^N \subseteq \mathbb{R}^N$, denote by $y(\mathbf{X}) := y(X_1, \ldots, X_N)$ a real-valued, square-integrable, measurable transformation on $(\Omega, \mathcal{F})$. Here, $y : \mathbb{A}^N \to \mathbb{R}$ represents a relevant function from a mathematical model, describing an output response of interest for a UQ problem. A major objective of UQ analysis is to estimate the probabilistic characteristics of an output random variable $Y = y(\mathbf{X})$, including statistical moments and reliability, when the probability law of the input random vector $\mathbf{X}$ is prescribed. More often than not, Y is assumed to belong to a reasonably large class of random variables, such as the weighted L^2 space

$$L^2(\Omega, \mathcal{F}, \mathbb{P}) := \left\{ Y : \Omega \to \mathbb{R} : \int_\Omega |y(\mathbf{X}(\omega))|^2 d\mathbb{P}(\omega) = \int_{\mathbb{A}^N} |y(\mathbf{x})|^2 f_{\mathbf{X}}(\mathbf{x}) d\mathbf{x} < \infty \right\},$$

which is a Hilbert space with the inner product

$$(y(\mathbf{X}), z(\mathbf{X}))_{L^2(\Omega,\mathcal{F},\mathbb{P})} := \int_\Omega y(\mathbf{X}(\omega)) z(\mathbf{X}(\omega)) d\mathbb{P}(\omega) = \int_{\mathbb{A}^N} y(\mathbf{x}) z(\mathbf{x}) f_{\mathbf{X}}(\mathbf{x}) d\mathbf{x}$$

and norm

$$\|y(\mathbf{X})\|_{L^2(\Omega,\mathcal{F},\mathbb{P})} := \sqrt{(y(\mathbf{X}), y(\mathbf{X}))_{L^2(\Omega,\mathcal{F},\mathbb{P})}} = \sqrt{\int_\Omega y^2(\mathbf{X}(\omega)) d\mathbb{P}(\omega)} = \sqrt{\int_{\mathbb{A}^N} y^2(\mathbf{x}) f_{\mathbf{X}}(\mathbf{x}) d\mathbf{x}}.$$

If there is more than one output variable, then each can be defined from a function y considered one at a time. Indeed, the generalization for a multivariate output random vector is straightforward.

3. Measure-consistent multivariate orthonormal polynomials

When $\mathbf{X} = (X_1, \ldots, X_N)^\intercal$ comprises statistically dependent random variables, the resultant probability measure, in general, is not a product-type, meaning that the joint distribution of $\mathbf{X}$ cannot be obtained strictly from its marginal distributions. Consequently, measure-consistent multivariate orthonormal polynomials in $\mathbf{x} = (x_1, \ldots, x_N)^\intercal$ cannot be built from an N-dimensional tensor product of measure-consistent univariate orthonormal polynomials. In this section, a method founded on a whitening transformation of the monomial basis is presented to generate multivariate orthonormal polynomials that are consistent with an arbitrary, non-product-type probability measure $f_{\mathbf{X}}(\mathbf{x})d\mathbf{x}$ of $\mathbf{X}$.

3.1. Monomial basis

Let $\mathbf{j} := (j_1, \ldots, j_N) \in \mathbb{N}_0^N$ be an N-dimensional multi-index. For $\mathbf{x} = (x_1, \ldots, x_N)^\intercal \in \mathbb{A}^N \subseteq \mathbb{R}^N$, a monomial in the real variables $x_1, \ldots, x_N$ is the product $\mathbf{x}^{\mathbf{j}} = x_1^{j_1} \cdots x_N^{j_N}$ and has a total degree $|\mathbf{j}| = j_1 + \cdots + j_N$. A linear combination of $\mathbf{x}^{\mathbf{j}}$, where $|\mathbf{j}| = l$, $l \in \mathbb{N}_0$, is a homogeneous polynomial of degree l. Define by

$$\mathcal{P}_l^N := \text{span}\{\mathbf{x}^{\mathbf{j}} : |\mathbf{j}| = l, \mathbf{j} \in \mathbb{N}_0^N\}, \ l \in \mathbb{N}_0,$$

the space of homogeneous polynomials of degree l and by

$$\Pi_m^N := \text{span}\{\mathbf{x}^{\mathbf{j}} : |\mathbf{j}| \le m, \mathbf{j} \in \mathbb{N}_0^N\}, \ m \in \mathbb{N}_0,$$

the space of polynomials of degree at most m. It is well known that the dimensions of the vector spaces $\mathcal{P}_l^N$ and Π_m^N are

$$\dim \mathcal{P}_l^N = \#\left\{\mathbf{j} \in \mathbb{N}_0^N : |\mathbf{j}| = l\right\} = \binom{N+l-1}{l}$$

and

$$\dim \Pi_m^N = \sum_{l=0}^{m} \dim \mathcal{P}_l^N = \sum_{l=0}^{m} \binom{N+l-1}{l} = \binom{N+m}{m} =: L_{N,m}, \tag{1}$$

respectively, where $L_{N,m}$ represents the dimension of Π_m^N.

Consider for each $m \in \mathbb{N}_0$ the elements of the multi-index set $\{\mathbf{j} \in \mathbb{N}_0^N : |\mathbf{j}| \le m\}$, which is arranged as $\mathbf{j}^{(1)}, \ldots, \mathbf{j}^{(L_{N,m})}$, $\mathbf{j}^{(1)} = \mathbf{0}$, according to a monomial order of choice. The set has cardinality $L_{N,m}$, as defined in (1). Denote by

$$\mathbf{P}_m(\mathbf{x}) = (\mathbf{x}^{\mathbf{j}^{(1)}}, \ldots, \mathbf{x}^{\mathbf{j}^{(L_{N,m})}})^\intercal$$

an $L_{N,m}$-dimensional column vector whose elements are the monomials $\mathbf{x}^{\mathbf{j}}$ for $|\mathbf{j}| \le m$ arranged in the aforementioned order. It is referred to as the monomial vector in $\mathbf{x} = (x_1, \ldots, x_N)^\intercal$ of degree at most m. It is well known that the set of elements obtained from $\mathbf{P}_m(\mathbf{x})$ constitutes a basis of Π_m^N.

3.2. Monomial moment matrix

When the input random variables $X_1, \ldots, X_N$, instead of the real variables $x_1, \ldots, x_N$, are inserted in the argument, $\mathbf{P}_m(\mathbf{X})$ becomes a vector of random monomials. This leads to an $L_{N,m} \times L_{N,m}$ monomial moment matrix of $\mathbf{P}_m(\mathbf{X})$, defined as

$$\mathbf{G}_m := \mathbb{E}[\mathbf{P}_m(\mathbf{X})\mathbf{P}_m^\intercal(\mathbf{X})] := \int_{\mathbb{A}^N} \mathbf{P}_m(\mathbf{x})\mathbf{P}_m^\intercal(\mathbf{x}) f_{\mathbf{X}}(\mathbf{x}) d\mathbf{x}, \tag{2}$$

with its (p, q)th element

$$G_{m,pq} := \mathbb{E}[\mathbf{X}^{\mathbf{j}^{(p)}}\mathbf{X}^{\mathbf{j}^{(q)}}] := \int_{\mathbb{A}^N} \mathbf{x}^{\mathbf{j}^{(p)}}\mathbf{x}^{\mathbf{j}^{(q)}} f_{\mathbf{X}}(\mathbf{x}) d\mathbf{x} = \int_{\mathbb{A}^N} \mathbf{x}^{\mathbf{j}^{(p)}+\mathbf{j}^{(q)}} f_{\mathbf{X}}(\mathbf{x}) d\mathbf{x}, \quad p, q = 1, \ldots, L_{N,m}. \tag{3}$$

When $m > 0$, $G_{m,pq}$ represents the expectation of a product of two random monomials of degree at most m. However, $\mathbf{G}_m$ is not a covariance matrix of $\mathbf{P}_m(\mathbf{X})$, as the means of random monomials are not *zero* in general. It is elementary to show that $\mathbf{G}_m$ is symmetric and positive-definite.

3.3. Whitening transformation

Given $m \in \mathbb{N}_0$ and the previously chosen monomial order, define by

$$\mathbf{\Psi}_m(\mathbf{x}) := (\Psi_{\mathbf{j}^{(1)}}(\mathbf{x}), \ldots, \Psi_{\mathbf{j}^{(L_{N,m})}}(\mathbf{x}))^\intercal := (\Psi_1(\mathbf{x}), \ldots, \Psi_{L_{N,m}}(\mathbf{x}))^\intercal \tag{4}$$

an $L_{N,m}$-dimensional column vector of orthonormal polynomials, which is consistent with the probability measure $f_{\mathbf{X}}(\mathbf{x})d\mathbf{x}$. Such polynomials can be generated from the monomial vector $\mathbf{P}_m$ and properties of the monomial moment matrix $\mathbf{G}_m$, where the orthonormality is addressed in Section 3.4. In (4), $\Psi_{\mathbf{j}^{(p)}}(\mathbf{x})$, $p = 1, \ldots, L_{N,m}$, represents the pth element of $\mathbf{\Psi}_m(\mathbf{x})$ consistent with the monomial order of choice, whereas, for simplicity, the subscript $\mathbf{j}^{(p)}$ has been replaced with p in the second equality to denote the same element. To construct such orthonormal polynomials, recognize that the monomial moment matrix $\mathbf{G}_m$, as it is symmetric and positive-definite, is invertible. Therefore, for each $m \in \mathbb{N}_0$, there exists a non-singular $L_{N,m} \times L_{N,m}$ whitening matrix $\mathbf{W}_m$, satisfying

$$\mathbf{W}_m^\intercal \mathbf{W}_m = \mathbf{G}_m^{-1} \quad \text{or} \quad \mathbf{W}_m^{-1}\mathbf{W}_m^{-\intercal} = \mathbf{G}_m. \tag{5}$$

Thereafter, apply a whitening transformation to create the orthonormal polynomial vector

$$\mathbf{\Psi}_m(\mathbf{x}) = \mathbf{W}_m \mathbf{P}_m(\mathbf{x}), \quad m \in \mathbb{N}_0, \tag{6}$$

from the known monomial vector $\mathbf{P}_m(\mathbf{x})$. The transformation is coined "whitening" because it changes one random vector to the other, which has statistical properties akin to that of a white noise vector. However, the whitening matrix $\mathbf{W}_m$ involved in (6) is not uniquely determined from the invertibility of $\mathbf{G}_m$. Indeed, there are multiple options to select $\mathbf{W}_m$, all fulfilling the condition described in (5).

A prominent choice of the whitening matrix involves Cholesky factorization [12], which leads to the following selection of

$$\mathbf{W}_m = \mathbf{Q}_m^{-1}, \quad \mathbf{G}_m = \mathbf{Q}_m \mathbf{Q}_m^\intercal. \tag{7}$$

Here, $\mathbf{Q}_m$ is an $L_{N,m} \times L_{N,m}$ real-valued lower-triangular matrix determined from the Cholesky factorization of $\mathbf{G}_m$. Interested readers are encouraged to review prior works [12,17] on additional choices for the whitening matrix.

It is important not to conflate the whitening transformation with measure transformations frequently used for mapping dependent variables to independent ones. The latter transformations are generally nonlinear for non-Gaussian variables. In contrast, the transformation introduced here is linear and maps monomials to orthonormal polynomials for any input probability measure. As long as the monomial moment matrix $\mathbf{G}_m$ exists and can be constructed, as discussed more in a forthcoming subsection, orthonormal polynomials consistent with a wide variety of dependent variables can be created.

3.4. First- and second-moment properties

When the input random variables are used as the argument, $\boldsymbol{\Psi}_m(\mathbf{X})$ becomes a vector of random orthonormal polynomials. Therefore, it is important to establish their second-moment properties, to be exploited in the next section.

Imposing the expectation operator on (6), the first-order moment of the orthonormal polynomial vector is

$$\begin{aligned}\mathbb{E}[\boldsymbol{\Psi}_m(\mathbf{X})] &= \mathbf{W}_m\mathbb{E}[\mathbf{P}_m(\mathbf{X})]\\ &= \mathbf{W}_m\mathbf{G}_m(1,0,\ldots,0)^\intercal\\ &= \mathbf{Q}_m^{-1}\mathbf{Q}_m\mathbf{Q}_m^\intercal(1,0,\ldots,0)^\intercal\\ &= \mathbf{Q}_m^\intercal(1,0,\ldots,0)^\intercal\\ &= (1,0,\ldots,0)^\intercal.\end{aligned} \tag{8}$$

Here, the second equality is attained from the cognizance that

$$\mathbb{E}[\mathbf{P}_m(\mathbf{X})] = \mathbf{G}_m\begin{pmatrix}1\\0\\\vdots\\0\end{pmatrix} = \mathbf{G}_m(1,0,\ldots,0)^\intercal,$$

whereas the last equality results from the fact that $\mathbf{Q}_m^\intercal$ is an upper-triangular matrix with the (1,1)th element being *one*.

According to (8), if the whitening matrix is selected from the Cholesky factorization, then the means of non-constant orthonormal polynomials vanish for any probability measure. However, the same cannot be said for other cases of whitening matrices not explicitly considered here.

Similarly, applying the expectation operator on the quadratic form of (6), the second-order moment of the orthonormal polynomial vector becomes

$$\begin{aligned}\mathbb{E}[\boldsymbol{\Psi}_m(\mathbf{X})\boldsymbol{\Psi}_m^\intercal(\mathbf{X})] &= \mathbb{E}[\mathbf{W}_m\mathbf{P}_m(\mathbf{X})\mathbf{P}_m^\intercal(\mathbf{X})\mathbf{W}_m^\intercal]\\ &= \mathbf{W}_m\mathbb{E}[\mathbf{P}_m(\mathbf{X})\mathbf{P}_m^\intercal(\mathbf{X})]\mathbf{W}_m^\intercal\\ &= \mathbf{W}_m\mathbf{G}_m\mathbf{W}_m^\intercal\\ &= \mathbf{W}_m\mathbf{W}_m^{-1}\mathbf{W}_m^{-\intercal}\mathbf{W}_m^\intercal\\ &= \mathbf{I}_m.\end{aligned} \tag{9}$$

The steps of (9) involve using the whitening transformation in (6), the definition of the monomial moment matrix $\mathbf{G}_m$ in (2), and the condition described in (5). As a result, an $L_{N,m}\times L_{N,m}$ identity matrix $\mathbf{I}_m$ is generated, proving orthonormality of the polynomial basis set.

Since no specific expression of $\mathbf{W}_m$ has been used, the resultant polynomial vector $\boldsymbol{\Psi}_m(\mathbf{X})$ is orthonormal for any choice of the whitening matrix. However, when $\mathbf{W}_m$ is obtained from the Cholesky factorization, the non-constant polynomials of $\boldsymbol{\Psi}_m(\mathbf{X})$ also become uncorrelated. These desirable properties produce concise expressions of GPCE statistics, to be explained in the following section.

For an ith element $\Psi_i(\mathbf{X})$ of the polynomial vector $\boldsymbol{\Psi}_m(\mathbf{X}) = (\Psi_1(\mathbf{X}),\ldots,\Psi_{L_{N,m}}(\mathbf{X}))^\intercal$, the first- and second-order moments are

$$\mathbb{E}[\Psi_i(\mathbf{X})] = \begin{cases}1, & \text{if } i=1,\\ 0, & \text{if } i\neq 1,\end{cases} \tag{10}$$

and

$$\mathbb{E}[\Psi_i(\mathbf{X})\Psi_j(\mathbf{X})] = \begin{cases}1, & i=j,\\ 0, & i\neq j,\end{cases} \tag{11}$$

respectively.

3.5. An illustrative example

Consider two ($N=2$) statistically dependent *zero*-mean Gaussian random variables X_1 and X_2 with identical standard deviations $\sigma_1=\sigma_2=1/4$ and correlation coefficient $\rho=9/10$. Set $m=2$ to generate at most second-order measure-consistent orthonormal polynomials in $\mathbf{x}=(x_1,x_2)^\intercal\in\mathbb{R}^2$.

From (1), $L_{2,2} = \binom{2+2}{2} = 6$, and the monomial vector, arranged according to the graded lexicographic order, is

$$\mathbf{P}_2(x_1, x_2) = (1, x_1, x_2, x_1^2, x_1x_2, x_2^2)^\intercal.$$

Moreover, the set of elements of $\mathbf{P}_2(x_1, x_2)$ is a basis of Π_2^2.

Using (2) and (7), the monomial moment matrix and whitening matrix are exactly calculated as

$$\mathbf{G}_2 = \begin{bmatrix} 1 & 0 & 0 & \frac{1}{16} & \frac{9}{160} & \frac{1}{16} \\ 0 & \frac{1}{16} & \frac{9}{160} & 0 & 0 & 0 \\ 0 & \frac{9}{160} & \frac{1}{16} & 0 & 0 & 0 \\ \frac{1}{16} & 0 & 0 & \frac{3}{256} & \frac{27}{2560} & \frac{131}{12800} \\ \frac{9}{160} & 0 & 0 & \frac{27}{2560} & \frac{131}{12800} & \frac{27}{2560} \\ \frac{1}{16} & 0 & 0 & \frac{131}{12800} & \frac{27}{2560} & \frac{3}{256} \end{bmatrix},$$

$$\mathbf{W}_2 = \begin{bmatrix} 1 & 0 & 0 & 0 & 0 & 0 \\ 0 & 4 & 0 & 0 & 0 & 0 \\ 0 & -\frac{36}{\sqrt{19}} & \frac{40}{\sqrt{19}} & 0 & 0 & 0 \\ -\frac{1}{\sqrt{2}} & 0 & 0 & 8\sqrt{2} & 0 & 0 \\ 0 & 0 & 0 & -\frac{144}{\sqrt{19}} & \frac{160}{\sqrt{19}} & 0 \\ -\frac{1}{\sqrt{2}} & 0 & 0 & \frac{648\sqrt{2}}{19} & -\frac{1440\sqrt{2}}{19} & \frac{800\sqrt{2}}{19} \end{bmatrix}.$$

Thereafter, (6) yields an orthonormal polynomial vector as

$$\boldsymbol{\Psi}_2(x_1, x_2) = \begin{pmatrix} 1 \\ 4x_1 \\ -\frac{36}{\sqrt{19}}x_1 + \frac{40}{\sqrt{19}}x_2 \\ -\frac{1}{\sqrt{2}} + 8\sqrt{2}x_1^2 \\ -\frac{144}{\sqrt{19}}x_1^2 + \frac{160}{\sqrt{19}}x_1x_2 \\ -\frac{1}{\sqrt{2}} + \frac{648\sqrt{2}}{19}x_1^2 - \frac{1440\sqrt{2}}{19}x_1x_2 + \frac{800\sqrt{2}}{19}x_2^2 \end{pmatrix}.$$

It is elementary to verify that these orthonormal polynomials satisfy the statistical properties described in (8)–(11). Unfortunately, measure-consistent orthonormal polynomials in general cannot be determined exactly for an arbitrary probability measure. They must, in such a case, be obtained numerically, to be explained further in Section 5.

4. Generalized polynomial chaos expansion

According to (9) or (11), any two distinct elements $\Psi_i(\mathbf{x})$ and $\Psi_j(\mathbf{x})$, $i, j = 1, \ldots, L_{N,m}$, of the polynomial vector $\boldsymbol{\Psi}_m(\mathbf{x})$ are mutually orthonormal. Therefore, the set $\{\Psi_i(\mathbf{x}), 1 \le i \le L_{N,m}\} \subset \Pi_m^N$, constructed from the elements of $\boldsymbol{\Psi}_m(\mathbf{x})$, is linearly independent. Moreover, the set has cardinality $L_{N,m}$, which matches the dimension of the polynomial space Π_m^N. Therefore, $\{\Psi_i(\mathbf{x}), 1 \le i \le L_{N,m}\}$ is a basis of Π_m^N, yielding

$$\Pi_m^N = \text{span}\{\Psi_i(\mathbf{x}), 1 \le i \le L_{N,m}\}, \quad m \in \mathbb{N}_0.$$

Given a fixed value of N, the size of the spanning set $\{\Psi_i(\mathbf{x}),\ 1 \le i \le L_{N,m}\}$ is controlled by the order m. The larger the value of m, the larger the value of $L_{N,m}$ and, hence, the size of the set. For a refinement process, consider increasing the value of m, resulting in an increasing family of the sets of such basis functions. In the limit, when $m \to \infty$, denote by $\{\Psi_i(\mathbf{x}),\ 1 \le i < \infty\}$ the resulting spanning set, consisting of an infinite number of basis functions. If the probability density function of random input $\mathbf{X}$ is compactly supported or is exponentially integrable, as mandated by Assumption 1, then it can be shown that the set of random orthonormal polynomials $\{\Psi_i(\mathbf{X}),\ 1 \le i < \infty\}$ forms an orthonormal basis of $L^2(\Omega, \mathcal{F}, \mathbb{P})$. Consequently,

$$L^2(\Omega, \mathcal{F}, \mathbb{P}) = \overline{\text{span}\{\Psi_i(\mathbf{X}),\ 1 \le i < \infty\}}, \tag{12}$$

where the overline represents set closure.

4.1. Fourier polynomial expansion

Given the important theoretical result in (12), the standard Hilbert space theory says that every random variable from $L^2(\Omega, \mathcal{F}, \mathbb{P})$ can be expanded in terms of the spanning set. The result is GPCE, formally presented as Theorem 1.

Theorem 1 [12]. *Let $\mathbf{X} := (X_1, \ldots, X_N)^\intercal$ be a vector of $N \in \mathbb{N}$ input random variables satisfying Assumption 1. Recall that $\{\Psi_i(\mathbf{X}),\ 1 \le i < \infty\}$, a set of multivariate orthonormal polynomials in $\mathbf{x}$, has been obtained consistent with the probability measure $f_{\mathbf{X}}(\mathbf{x})d\mathbf{x}$. Then any random variable $y(\mathbf{X}) \in L^2(\Omega, \mathcal{F}, \mathbb{P})$ can be expanded as a Fourier series comprising multivariate orthonormal polynomials in $\mathbf{X}$, referred to as the GPCE of*

$$y(\mathbf{X}) \sim \sum_{i=1}^{\infty} C_i \Psi_i(\mathbf{X}),$$

where the expansion coefficients $C_i \in \mathbb{R},\ i = 1, \ldots, \infty$, are defined as

$$C_i = \mathbb{E}[y(\mathbf{X})\Psi_i(\mathbf{X})] := \int_{\mathbb{A}^N} y(\mathbf{x})\Psi_i(\mathbf{x}) f_{\mathbf{X}}(\mathbf{x}) d\mathbf{x},\ \ i = 1, \ldots, \infty. \tag{13}$$

Moreover, the GPCE of $y(\mathbf{X}) \in L^2(\Omega, \mathcal{F}, \mathbb{P})$ converges in mean-square, in probability, and in distribution. Here, the symbol $\sim$ represents equality in a weaker sense, such as equality in mean-square, but not necessarily pointwise, nor almost everywhere.

The proof is omitted here, as it is available elsewhere [12].

4.2. GPCE approximation

The GPCE contains an infinite number of orthonormal polynomials or coefficients. In a practical setting, the number must be finite, meaning that the GPCE must be truncated. However, there are multiple ways to perform a truncation, such as those involving tensor-product, total-degree, and hyperbolic-cross index sets. In this work, the truncation stemming from the total-degree index set is adopted, which entails retaining polynomial expansion orders less than or equal to $m \in \mathbb{N}_0$. The result is an mth-order GPCE approximation

$$y_m(\mathbf{X}) = \sum_{i=1}^{L_{N,m}} C_i \Psi_i(\mathbf{X}) \tag{14}$$

of $y(\mathbf{X})$, which contains

$$L_{N,m} = \binom{N+m}{m} = \frac{(N+m)!}{N!m!} \tag{15}$$

number of expansion coefficients defined by (13).

4.3. Second-moment analysis

The mth-order GPCE approximation $y_m(\mathbf{X})$ can be viewed as an inexpensive surrogate of an expensive-to-calculate function $y(\mathbf{X})$. Therefore, relevant statistical properties of $y(\mathbf{X})$, such as its first two moments, can be estimated from those of $y_m(\mathbf{X})$.

Applying the expectation operator on $y_m(\mathbf{X})$ in (14) and recognizing (10), its mean

$$\mathbb{E}[y_m(\mathbf{X})] = C_1 = \mathbb{E}[y(\mathbf{X})] \tag{16}$$

matches the exact mean of $y(\mathbf{X})$ for any $m \in \mathbb{N}_0$. Enforcing the expectation operator again, this time on $(y_m(\mathbf{X}) - \mathbb{E}[y_m(\mathbf{X})])^2$, and using (11) results in the variance

$$\text{var}[y_m(\mathbf{X})] = \sum_{i=1}^{L_{N,m}} C_i^2 - C_1^2 = \sum_{i=2}^{L_{N,m}} C_i^2 \le \text{var}[y(\mathbf{X})] \tag{17}$$

of $y_m(\mathbf{X})$. Therefore, the second-moment statistics of a GPCE approximation are solely determined by an appropriately truncated set of expansion coefficients. The formulae (16) and (17) for the mean and variance of the GPCE approximation are the same as those established for the classical tensor-product PCE approximation, although the respective expansion coefficients involved are not. The fundamental reason for this resemblance is rooted in the use of an orthonormal polynomial basis in both expansions.

4.4. Reliability analysis

A fundamental problem in reliability analysis entails calculation of the failure probability

$$P_F := \mathbb{P}[\mathbf{X} \in \Omega_F] = \int_{\mathbb{A}^N} I_{\Omega_F}(\mathbf{x}) f_{\mathbf{X}}(\mathbf{x}) d\mathbf{x} =: \mathbb{E}\left[I_{\Omega_F}(\mathbf{X})\right], \tag{18}$$

where $I_{\Omega_F}(\mathbf{x})$ is the indicator function associated with the failure domain Ω_F, which is equal to *one* when $\mathbf{x} \in \Omega_F$ and *zero* otherwise. For a component reliability analysis, the failure domain is often adequately described by a single performance function $y(\mathbf{X})$, for instance, $\Omega_F := \{\mathbf{x}: y(\mathbf{x}) < 0\}$, whereas multiple, interdependent performance functions are required for a system reliability analysis. In this work, only component reliability analysis is considered.

Let $\Omega_{F,m} := \{\mathbf{x}: y_m(\mathbf{x}) < 0\}$ be an approximate failure set as a result of an mth-order GPCE approximation $y_m(\mathbf{X})$ of $y(\mathbf{X})$. Then, an estimate of the failure probability P_F in (18), obtained using MCS of the GPCE approximation, is

$$P_{F,m} = \mathbb{E}\left[I_{\Omega_{F,m}}(\mathbf{X})\right] = \lim_{L' \to \infty} \frac{1}{L'} \sum_{l=1}^{L'} I_{\Omega_{F,m}}(\mathbf{x}^{(l)}), \tag{19}$$

where L' is the sample size of the GPCE approximation, $\mathbf{x}^{(l)}$ is the lth realization of $\mathbf{X}$, and $I_{\Omega_{F,m}}(\mathbf{x})$ is another indicator function, which is equal to *one* when $\mathbf{x} \in \Omega_{F,m}$ and *zero* otherwise.

Note that the simulation of the GPCE approximation in (19) should not be confused with the standard MCS commonly used for producing benchmark results. The standard MCS, which requires numerical calculations of $y(\mathbf{x}^{(l)})$ for input samples $\mathbf{x}^{(l)}$, $l = 1, \ldots, L_{MCS}$, $L_{MCS} \in \mathbb{N}$, can be expensive or even prohibitive, particularly when the sample size L_{MCS} needs to be very large for estimating small failure probabilities. In contrast, the MCS embedded in the GPCE approximation requires evaluations of simple polynomial functions that describe $y_m(\mathbf{x}^{(l)})$. Therefore, a relatively large sample size ($L' \gg L_{MCS}$) can be accommodated in the GPCE approximation even when y is expensive to evaluate.

5. Generation of orthonormal polynomials

For a random input $\mathbf{X}$ following an arbitrary probability measure $f_{\mathbf{X}}(\mathbf{x})d\mathbf{x}$, the expectation in (3), which involves multi-dimensional integration, cannot be calculated analytically or exactly. In other words, only an estimate $\tilde{\mathbf{G}}_m$ of the monomial moment matrix $\mathbf{G}_m$ can be attained in a practical setting. As a result, an approximate version of the mth-order orthonormal polynomial vector, denoted by $\tilde{\boldsymbol{\Psi}}_m(\mathbf{x})$, is generated instead.

5.1. Construction of approximate monomial moment matrix

The assembly of $\tilde{\mathbf{G}}_m$ poses a few challenges of its own. In this work, two classes of methods, one stemming from numerical integration and the other rooted in sampling methods, are proposed to construct the monomial moment matrix approximately.

5.1.1. Numerical integration

A natural inclination is to estimate the expectation in (3) by numerical integration, for instance, by Gauss quadrature or cubature. However, there may not exist a Gauss quadrature rule for a general non-product-type probability measure. To overcome this quandary, two options, depending on the shape of the domain $\mathbb{A}^N$, are suggested.

Option 1. The first option, applicable to a rectangular or non-rectangular domain $\mathbb{A}^N \subseteq \mathbb{R}^N$, constitutes a general approach. It entails a change of variables from $\mathbf{x} = (x_1, \ldots, x_N)$ to $\mathbf{z} = (z_1, \ldots, z_N)$ (say), where z_i is a realization of a continuous independent random variable Z_i, which has absolutely continuous probability distribution function $F_{Z_i}(z_i) := \mathbb{P}[Z_i \le z_i]$ and continuous probability density function $f_{Z_i}(z_i) := \partial F_{Z_i}(z_i)/\partial z_i$ supported on a bounded or an unbounded interval $[a_i, b_i] \subseteq \mathbb{R}$, $a_i, b_i \in \mathbb{R}$, $b_i > a_i$, $i = 1, \ldots, N$. For instance, the change of variables from the Rosenblatt transformation [10] is

$$\begin{aligned} x_1 &= F_{X_1}^{-1}[F_{Z_1}(z_1)] \\ x_2 &= F_{X_2|X_1}^{-1}[F_{Z_2}(z_2)|x_1] \\ &\vdots \\ x_N &= F_{X_N|X_1,\ldots,X_{N-1}}^{-1}[F_{Z_N}(z_N)|x_1, \ldots, x_{N-1}], \end{aligned} \tag{20}$$

where $F_{X_1}(x_1) := \mathbb{P}[X_1 \le x_1]$ is the marginal distribution function of X_1 and

$$F_{X_i|X_1,\ldots,X_{i-1}}(x_i) := \mathbb{P}[X_i \le x_i | X_1 = x_1, \ldots, X_{i-1} = x_{i-1}], \quad i = 2, \ldots, N,$$

is a conditional distribution function of X_i. Then, using (20) in (3), the expectation becomes

$$\begin{aligned} G_{m,pq} &:= \int_{\mathbb{A}^N} x_1^{j_1^{(p)}+j_1^{(q)}} \cdots x_N^{j_N^{(p)}+j_N^{(q)}} f_{\mathbf{X}}(\mathbf{x}) d\mathbf{x} \\ &= \int_{\times_{i=1}^N [a_i,b_i]} x_1^{j_1^{(p)}+j_1^{(q)}} \cdots x_N^{j_N^{(p)}+j_N^{(q)}} \frac{f_{Z_1}(z_1)\cdots f_{Z_N}(z_N)}{f_{\mathbf{X}}(\mathbf{x})} f_{\mathbf{X}}(\mathbf{x}) d\mathbf{z} \\ &= \int_{\times_{i=1}^N [a_i,b_i]} x_1^{j_1^{(p)}+j_1^{(q)}} \cdots x_N^{j_N^{(p)}+j_N^{(q)}} f_{Z_1}(z_1)\cdots f_{Z_N}(z_N) dz_1 \cdots dz_N, \end{aligned} \tag{21}$$

where the fractional term in the integrand of the second line is the determinant of the Jacobian of the transformation and the monomial in the integrand is a function of $\mathbf{z}$, as described in (20). Compared with (3), which represents an N-dimensional integral on a possibly non-rectangular domain $\mathbb{A}^N$, the last line of (21) is an N-dimensional integral on a rectangular domain $\times_{i=1}^N [a_i, b_i]$ with a separable density function as the kernel. Still, an exact evaluation of the integral is impossible for a general probability measure of $\mathbf{X}$, suggesting a need for numerical approximation. Henceforth, a general anisotropic $(n_1, \ldots, n_N)$-point, multivariate, tensor-product Gauss-type quadrature rule yields an estimate

$$\tilde{G}_{m,pq} = \underbrace{\sum_{k_1=1}^{n_1} \cdots \sum_{k_N=1}^{n_N}}_{N \text{ sums}} \left(x_1^{(k_1)}\right)^{j_1{}^{(p)}+j_1{}^{(q)}} \cdots \left(x_N^{(k_N)}\right)^{j_N{}^{(p)}+j_N{}^{(q)}} \prod_{i=1}^N w_i^{(k_i)}, \tag{22}$$

of $G_{m,pq}$, where

$$x_i^{(k_i)} = \begin{cases} F_{X_1}^{-1}[F_{Z_1}(z_1^{(k_1)})], & i = 1, \\ F_{X_i|X_1,\ldots,X_{i-1}}^{-1}[F_{Z_i}(z_i^{(k_i)}) | x_1^{(k_1)}, \ldots, x_{i-1}^{(k_{i-1})}], & i = 2, \ldots, N, \end{cases}$$

and, for each $i = 1, \ldots, N$, $z_i^{(k_i)}$ and $w_i^{(k_i)}$ are integration points and matching weights, respectively, with k_i running from 1 to $n_i \in \mathbb{N}$. The integration points and associated weights depend on the probability measure $f_{Z_i}(z_i)dz_i$ of Z_i and are readily available, such as the Stieltjes procedure [11,18], to generate the measure-consistent Gauss quadrature formulae. If the density functions of Z_i are identical and $n_1 = \cdots = n_N = n$ (say), then the result is an n-point isotropic quadrature rule.

It is important to recognize that the Rosenblatt transformation, depending on the choice of transformed variables $\mathbf{z} = (z_1, \ldots, z_N)$, may result in a highly nonlinear integrand. As a result, a high-order Gauss quadrature rule is often required to be able to estimate the integral with high precision. Therefore, for computational expediency, selecting $\mathbf{Z}$ with a distribution close to that of $\mathbf{X}$ is recommended. This issue will be clarified when presenting a numerical example.

Option 2. The second option, simpler than the first one, is relevant when $\mathbb{A}^N \subseteq \mathbb{R}^N$ is a rectangular domain. It involves factoring the integrand with a chosen positive weight function, say, $w(\mathbf{x})$ on $\mathbb{A}^N$, for which a Gauss quadrature rule is readily available. In that case, (3) can be rewritten as

$$G_{m,pq} = \int_{\mathbb{A}^N} \mathbf{x}^{\mathbf{j}^{(p)}+\mathbf{j}^{(q)}} \frac{f_{\mathbf{X}}(\mathbf{x})}{w(\mathbf{x})} w(\mathbf{x}) d\mathbf{x}, \tag{23}$$

followed by a Gauss quadrature approximation of $G_{m,pq}$ in coherence with the weight function. The simplest example is selecting a constant weight function uniformly distributed over $\mathbb{A}^N$ and then exploiting the multivariate Gauss–Legendre quadrature rule to approximate the integral. However, as the integrand

$$\mathbf{x}^{\mathbf{j}^{(p)}+\mathbf{j}^{(q)}} \frac{f_{\mathbf{X}}(\mathbf{x})}{w(\mathbf{x})}$$

of (23) may no longer be a polynomial, a high-order Gauss quadrature is warranted for an acceptable error. Clearly, the quality of the approximation depends on the weight function. An optimal selection is desirable, but it is hardly trivial for a general probability measure. Here, the authors propose to obtain the weight function as the product of marginal probability density functions $f_{X_i}(x_i)$ of input random variables, that is,

$$w(\mathbf{x}) = \prod_{i=1}^N f_{X_i}(x_i). \tag{24}$$

In doing so, the resultant Gauss quadrature rule reproduces the exact value of $G_{m,pq}$ for, at least, a product-type probability measure of input variables. The motivation is that the integrand of (23) with the weight function in (24) is better approximated by polynomials than that obtained using the uniformly distributed constant weight function. Hereafter, a general

anisotropic $(n_1, \ldots, n_N)$-point, multivariate, tensor-product Gauss-type quadrature rule yields another estimate

$$\tilde{G}'_{m,pq} = \underbrace{\sum_{k_1=1}^{n_1} \cdots \sum_{k_N=1}^{n_N}}_{N \text{ sums}} \left(x_1^{(k_1)}\right)^{j_1{}^{(p)}+j_1{}^{(q)}} \cdots \left(x_N^{(k_N)}\right)^{j_N{}^{(p)}+j_N{}^{(q)}} \frac{f_{\mathbf{X}}(x_1^{(k_1)}, \ldots, x_N^{(k_N)})}{\prod_{i=1}^N f_{X_i}(x_i^{(k_i)})} \prod_{i=1}^N w_i^{(k_i)}, \tag{25}$$

of $G_{m,pq}$, where $x_i^{(k_i)}$ and $w_i^{(k_i)}$ are integration points and associated weights, respectively, obtained consistent with the probability measure $f_{X_i}(x_i)dx_i$ of X_i. Similarly, if all marginal density functions are identical and $n_1 = \cdots = n_N = n$ (say), then the result is an n-point isotropic quadrature rule. Moreover, if $f_{\mathbf{X}}(\mathbf{x}) = \prod_{i=1}^N f_{X_i}(x_i)$, then an $(m+1)$-point isotropic Gauss quadrature rule exactly calculates $G_{m,pq}$.

For both options, the appropriate values of n_i depend on m and $f_{Z_i}(z_i)$ or $f_{X_i}(x_i)$. The larger the value of m, the larger the values of n_i required. When $n_i \to \infty$, $i = 1, \ldots, N$, $\tilde{G}_{m,pq}$ in (22) and $\tilde{G}'_{m,pq}$ in (25) both approach $G_{m,pq}$, ensuring convergence.

For a high-dimensional UQ problem, say, with N exceeding 10, evaluating the N-dimensional sum in (22) or (25) is tedious, but is not computationally prohibitive. This is because no generally expensive output function evaluations from finite element analysis (FEA) or other numerical simulations are involved. Indeed, the numerical integration can be performed with an arbitrary precision even when N is large.

5.1.2. Sampling methods

An alternative to Gauss quadrature is a sampling method, such as standard MCS and quasi MCS (QMCS), to estimate the expectation in (3). Here, the expectation or integral is expressed as the average of the integrand evaluated at a pseudo-random or a quasi-random sequence of points.

The sampling methods involve three principal steps:

(1) Select a sample size $L'' \in \mathbb{N}$ and generate a point set $\mathcal{P}_{L''} := \{\mathbf{z}^{(l)} \in [0,1]^N,\ l = 1, \ldots, L''\}$ consisting of L'' samples. Depending on whether MCS or QMCS is used, $\mathcal{P}_L$ represents either a randomly distributed point set or a low-discrepancy point set.
(2) Apply the Rosenblatt transformation [10] or others to map each sample $\mathbf{z}^{(l)} \in [0,1]^N$ from $\mathcal{P}_{L''}$ to a sample $\mathbf{x}^{(l)} = (x_1^{(l)}, \ldots, x_N^{(l)}) \in \mathbb{A}^N$ of $\mathbf{X}$, following the known probability measure $f_{\mathbf{X}}(\mathbf{x})d\mathbf{x}$.
(3) Approximate the expectation or integral in (3) as an arithmetic average of the integrand values at the aforementioned point set, resulting in yet another estimate

$$\tilde{G}''_{m,pq} = \frac{1}{L''} \sum_{l=1}^{L''} \left(\mathbf{x}^{(l)}\right)^{\mathbf{j}^{(p)}+\mathbf{j}^{(q)}} = \frac{1}{L''} \sum_{l=1}^{L''} \left(x_1^{(l)}\right)^{j_1^{(p)}+j_1^{(q)}} \cdots \left(x_N^{(l)}\right)^{j_N^{(p)}+j_N^{(q)}} \tag{26}$$

of $G_{m,pq}$.

From the strong law of large numbers, $\tilde{G}''_{m,pq}$ in (26) converges to $G_{m,pq}$ when $L'' \to \infty$.

Standard MCS provides a convergence rate of $\mathcal{O}(L''^{-1/2})$, which is independent of the stochastic dimension N. Therefore, it is ideally suited to high-dimensional UQ problems. But the price is slow convergence of standard MCS. In contrast, the convergence rate of QMCS is $\mathcal{O}((\log L'')^N L''^{-1})$. Therefore, N or L'' needs to be sufficiently small or large for QMCS to produce a faster convergence rate than standard MCS. Moreover, the convergence rate of QMCS depends on the quality of a low-discrepancy point set. According to Morokoff and Caflisch [19], QMCS is generally more accurate than standard MCS for smooth integrands, and QMCS associated with the Sobol sequence [20] outperforms others in high dimensions.

In summary, three different estimates of $G_{m,pq} - \tilde{G}_{m,pq}$ and $\tilde{G}'_{m,pq}$ by numerical integration and $\tilde{G}''_{m,pq}$ by sampling methods — have been proposed. All three estimates will be employed in numerical examples, to be further discussed in Section 8.

5.2. A three-step algorithm

For a general UQ problem entailing N input random variables, there are three main steps to the generation of an mth-order approximate measure-consistent orthonormal polynomial vector $\tilde{\boldsymbol{\Psi}}_m(\mathbf{x})$ of dimension $L_{N,m}$:

(1) Given $m \in \mathbb{N}_0$, create an mth-order monomial basis vector $\mathbf{P}_m(\mathbf{x})$ of dimension $L_{N,m}$.
(2) Construct the $L_{N,m} \times L_{N,m}$ approximate monomial moment matrix $\tilde{\mathbf{G}}_m$ using either numerical integration described in Section 5.1.1 or sampling methods described in Section 5.1.2.
(3) Select the $L_{N,m} \times L_{N,m}$ approximate whitening matrix $\tilde{\mathbf{W}}_m$ from the Cholesky decomposition of the approximate monomial moment matrix $\tilde{\mathbf{G}}_m$ attained in step 2, followed by the whitening transformation to generate approximate orthonormal polynomials from $\tilde{\boldsymbol{\Psi}}_m(\mathbf{x}) = \tilde{\mathbf{W}}_m \mathbf{P}_m(\mathbf{x})$.

The first step is elementary, as the monomial basis vector $\mathbf{P}_m(\mathbf{x})$ does not depend on the input probability measure. It is easily created exactly from the set of monomials $\{\mathbf{x}^{\mathbf{j}},\ |\mathbf{j}| \le m\}$, as soon as the order of monomials is picked. The last step is not difficult either, as it entails using standard methods of linear algebra and Cholesky factorization and then performing a

matrix-vector multiplication to generate the approximate orthonormal polynomial vector $\tilde{\boldsymbol{\Psi}}_m(\mathbf{x})$. The major work, relatively speaking, is in the second step, which involves building the approximate monomial moment matrix $\tilde{\mathbf{G}}_m$.

The success of the three-step algorithm is predicated on faithful construction of a well-conditioned monomial moment matrix, enabling Cholesky factorization by standard procedures of linear algebra. Although two distinct classes of methods have been proposed, caution should be exercised when the order m is exceedingly large. This is because the condition number of the monomial moment matrix, which is a Gram matrix, grows quickly with respect to m [21]. In a practical setting, though, m is typically less than four or five. In such cases, Cholesky factorization of the monomial moment matrix can be performed without much hardship.

6. Calculation of expansion coefficients

The evaluation of the expansion coefficients C_i, $i = 1, \ldots, L_{N,m}$, of an mth-order GPCE approximation $y_m(\mathbf{X})$ involves various high-dimensional integrations. For an arbitrary function y and an arbitrary probability distribution of random input $\mathbf{X}$, an exact evaluation of these coefficients from the definition alone is infeasible, if not impossible. Numerical integration involving a multivariate, tensor-product Gauss-type quadrature rule is computationally formidable and likely prohibitive for high-dimensional UQ problems. To surmount this hurdle, two regression methods, based on the data size relative to the number of coefficients, are proposed to obtain associated estimates $\tilde{C}_i$, $i = 1, \ldots, L_{N,m}$, of the coefficients.

The regression methods are predicated on the optimal approximation quality of the GPCE approximation. Recall that Π_m^N is a subspace of all polynomials in $\mathbf{X}$ which have orders at most m, including constants. Then the mth-order GPCE approximation $y_m(\mathbf{X})$, among all possible candidates from Π_m^N, is the best approximation of $y(\mathbf{X})$ in the sense that

$$\mathbb{E}[y(\mathbf{X}) - y_m(\mathbf{X})]^2 = \inf_{\bar{y}_m \in \Pi_m^N} \mathbb{E}[y(\mathbf{X}) - \bar{y}_m(\mathbf{X})]^2.$$

Thereafter, the approximate expansion coefficients of $y_m(\mathbf{X})$ are determined from the minimization of

$$\mathbb{E}\left[y(\mathbf{X}) - \sum_{i=1}^{L_{N,m}} \tilde{C}_i \tilde{\Psi}_i(\mathbf{X}) \right]^2, \tag{27}$$

where $\tilde{\Psi}_i(\mathbf{X})$, $i = 1, \ldots, L_{N,m}$, are approximate orthonormal polynomials in $\mathbf{X}$, generated as explained in Section 5.

6.1. Initial setup for general regression analysis

Given a UQ problem with known distribution of random input $\mathbf{X}$ and an output function $y : \mathbb{A}^N \to \mathbb{R}$, consider an input-output data set $\{\mathbf{x}^{(l)}, y(\mathbf{x}^{(l)})\}_{l=1}^{L}$ of size $L \in \mathbb{N}$. The mapping y can be as simple as an explicitly defined mathematical function or as intricate as an implicitly described function obtained via computational simulation, such as FEA of complex mechanical systems. In either case, the data set, often referred to as the experimental design, can be generated by calculating the function $y(\mathbf{x}^{(l)})$ at each input data $\mathbf{x}^{(l)}$. Various sampling methods, namely, standard MCS, QMCS, and Latin hypercube sampling, can be used to build the experimental design. A study on regression analysis using an MCS-generated data set was reported by Owen [22].

The objective of a regression analysis is to determine the approximate coefficients $\tilde{C}_i$, $i = 1, \ldots, L_{N,m}$, of an mth-order GPCE approximation $y_m(\mathbf{X})$ from the linear equations

$$\sum_{i=1}^{L_{N,m}} \tilde{C}_i \tilde{\Psi}_i(\mathbf{x}^{(l)}) = y(\mathbf{x}^{(l)}), \quad l = 1, \ldots, L. \tag{28}$$

Denote by

$$\mathbf{A} := \begin{bmatrix} \tilde{\Psi}_1(\mathbf{x}^{(1)}) & \cdots & \tilde{\Psi}_{L_{N,m}}(\mathbf{x}^{(1)}) \\ \vdots & \ddots & \vdots \\ \tilde{\Psi}_1(\mathbf{x}^{(L)}) & \cdots & \tilde{\Psi}_{L_{N,m}}(\mathbf{x}^{(L)}) \end{bmatrix}, \quad \mathbf{b} := (y(\mathbf{x}^{(1)}), \ldots, y(\mathbf{x}^{(L)}))^\intercal, \quad \text{and} \quad \mathbf{c} := (\tilde{C}_1, \ldots, \tilde{C}_{L_{N,m}})^\intercal$$

an $L \times L_{N,m}$ matrix comprising values of polynomial basis functions at data points, an L-dimensional column vector containing values of output function at data points, and an $L_{N,m}$-dimensional column vector of unknown expansion coefficients, respectively. Then the linear system (28) has the matrix form

$$\mathbf{A}\mathbf{c} = \mathbf{b}. \tag{29}$$

There are two primary considerations when performing regression to estimate the GPCE coefficients. First, when the data size is larger than the number of coefficients, that is, when $L > L_{N,m}$, (28) or (29) is an overdetermined system for which the standard least-squares (SLS) regression can be readily applied to estimate the coefficients. Second, when the data size is smaller than the number of coefficients, that is, when $L < L_{N,m}$, the result is an underdetermined system and SLS becomes invalid because the resulting information matrix does not have full rank. In that case, diffeomorphic modulation under

observable response preserving homotopy (D-MORPH) regression or others is desirable to improve the approximation quality of regression without sacrificing fitting accuracy [23]. In the remainder of this section, both SLS regression and a new variant of D-MORPH regression, referred to as partitioned D-MORPH regression, are described.

6.2. SLS Regression

According to SLS, the expansion coefficients of GPCE are estimated by minimizing

$$\hat{e}_m := \frac{1}{L}\sum_{l=1}^{L}\left[y(\mathbf{x}^{(l)}) - \sum_{j=1}^{L_{N,m}}\tilde{C}_j\tilde{\Psi}_j(\mathbf{x}^{(l)})\right]^2, \tag{30}$$

the empirical analog of (27). Performing differentiation on both sides of (30) with respect to $\tilde{C}_i$ and then setting it equal to *zero* yields

$$\sum_{j=1}^{L_{N,m}}\hat{C}_j\sum_{l=1}^{L}\tilde{\Psi}_j(\mathbf{x}^{(l)})\tilde{\Psi}_i(\mathbf{x}^{(l)}) = \sum_{l=1}^{L}y(\mathbf{x}^{(l)})\tilde{\Psi}_i(\mathbf{x}^{(l)}),\ \ i=1,\ldots,L_{N,m}. \tag{31}$$

Here, the solution $\hat{C}_i,\ i=1\ldots,L_{N,m}$, is obtained from the minimization of (30). In matrix form, the linear system (31) becomes

$$\mathbf{A}^\intercal\mathbf{A}\hat{\mathbf{c}} = \mathbf{A}^\intercal\mathbf{b}, \tag{32}$$

where $\hat{\mathbf{c}} := (\hat{C}_1,\ldots,\hat{C}_{L_{N,m}})^\intercal$ and the $L_{N,m}\times L_{N,m}$ matrix $\mathbf{A}^\intercal\mathbf{A}$ is known sometimes as the information or data matrix. On inversion, (32) yields the desired solution

$$\hat{\mathbf{c}} = (\mathbf{A}^\intercal\mathbf{A})^{-1}\mathbf{A}^\intercal\mathbf{b}$$

for the estimated coefficients by SLS. A necessary condition for the inversion is $L > L_{N,m}$. Even when the condition is satisfied, the experimental design must be judiciously selected in such a way that the matrix $\mathbf{A}^\intercal\mathbf{A}$ is well-conditioned.

It is unclear what the required or optimal factor $L/L_{N,m}$ is for the SLS regression method to be successful. Factors ranging from two to three have been reported for satisfactory estimates [24], but the authors suspect such factors to be too optimistic if a hard enough random variable is chosen from $L^2(\Omega,\mathcal{F},\mathbb{P})$. Nonetheless, if L is much larger than $L_{N,m}$, then the SLS regression method will not be feasible, as the computational price is directly proportional to L for UQ problems mandating expensive-to-evaluate output functions. Therefore, there is a need for alternative methods that are able to deal with smaller values of L, including when $L < L_{N,m}$, in providing satisfactory estimates of the coefficients.

6.3. Partitioned D-MORPH regression

The D-MORPH regression method was primarily developed for an underdetermined system where the data size is smaller than the number of coefficients. While Li and Rabitz [23] provide all the necessary details of the method, the basic steps of the original D-MORPH regression are briefly summarized here to aid in a self-contained description of the proposed partitioned D-MORPH that follows. Unlike the existing D-MORPH, the partitioned D-MORPH is applicable whether $L < L_{N,m}$ or $L > L_{N,m}$.

6.3.1. Original D-MORPH

For a linear regression problem with $L < L_{N,m}$, there exist an infinite number of solutions for $\mathbf{c}$, all satisfying (29). Collect these solutions to form a manifold $\mathcal{M}\subset\mathbb{R}^{L_{N,m}}$. Then the D-MORPH regression is applied to attain the best possible solution $\mathbf{c}\in\mathcal{M}$ by minimizing certain undesirable properties, which is analogous to regularized least-squares that controls the trade-off between overfitting and prediction accuracy. For $t\in\mathbb{R}_0^+$, denote by $\mathbf{a}(t)$ an exploration path and by $\mathbf{u}(t)$ an arbitrary vector in $\mathbb{R}^{L_{N,m}}$. Given the linear system (29), the family of possible solutions in $\mathcal{M}$ is written as [23]

$$\mathbf{a}(t) = \mathbf{A}^+\mathbf{b} + (\mathbf{I}_{L_{N,m}} - \mathbf{A}^+\mathbf{A})\mathbf{u}(t), \tag{33}$$

where $\mathbf{a}(t) = (a_1(t),\ldots,a_{L_{N,m}}(t))^\intercal$ with $a_i(t)\in\mathbb{R},\ i=1,\ldots,L_{N,m}$, representing possible solutions of approximate GPCE coefficients and $\mathbf{A}^+\in\mathbb{R}^{L_{N,m}\times L}$ is a generalized inverse of $\mathbf{A}\in\mathbb{R}^{L\times L_{N,m}}$, often preferred to satisfy the four well-known Moore-Penrose conditions [25]:

$$(1)\ \mathbf{A}\mathbf{A}^+\mathbf{A}=\mathbf{A},\ \ (2)\ \mathbf{A}^+\mathbf{A}\mathbf{A}^+=\mathbf{A}^+,\ \ (3)\ (\mathbf{A}\mathbf{A}^+)^\intercal=\mathbf{A}\mathbf{A}^+,\ \ (4)\ (\mathbf{A}^+\mathbf{A})^\intercal=\mathbf{A}^+\mathbf{A}.$$

For a real-valued full-rank or deficient matrix $\mathbf{A}$ with its row rank $r\le L$, such a generalized inverse, known as the Moore-Penrose inverse, is obtained from the matrix factorization

$$\mathbf{A}^+ = \mathbf{K}\begin{bmatrix}\mathbf{R}_r^{-1} & \mathbf{0}\\ \mathbf{0} & \mathbf{0}\end{bmatrix}\mathbf{H}^\intercal, \tag{34}$$

where $\mathbf{H}$ and $\mathbf{K}$ are $L \times L$ and $L_{N,m} \times L_{N,m}$ orthogonal matrices, respectively, and $\mathbf{R}_r$ is a nonsingular $r \times r$ diagonal matrix. They are easily obtained from the singular value decomposition of

$$\mathbf{A} = \mathbf{H}\begin{bmatrix}\mathbf{R}_r & \mathbf{0}\\ \mathbf{0} & \mathbf{0}\end{bmatrix}\mathbf{K}^{\intercal}.$$

If, however, $\mathbf{A}$ has a full row rank, that is, if $r = L$, then (34) is unnecessary because $\mathbf{A}^{+}$ can be computed directly from

$$\mathbf{A}^{+} = \mathbf{A}^{\intercal}(\mathbf{A}\mathbf{A}^{\intercal})^{-1}.$$

Coming back to (33), the first part of the solution $\mathbf{A}^{+}\mathbf{b}$ is the initial solution akin to the SLS solution, whereas the final solution, yet to be formulated, is generated from the D-MORPH regression.

In reference to (33), define

$$\mathbf{\Phi} := (\mathbf{I}_{L_{N,m}} - \mathbf{A}^{+}\mathbf{A}) \in \mathbb{R}^{L_{N,m}\times L_{N,m}} \text{ and } \mathbf{v}(t) := \frac{d\mathbf{u}(t)}{dt} \in \mathbb{R}^{L_{N,m}}, \tag{35}$$

where the latter represents a free function vector. Differentiating (33) with respect to t, with (35) in mind, produces

$$\frac{d\mathbf{a}(t)}{dt} = \mathbf{\Phi}\frac{d\mathbf{u}(t)}{dt} = \mathbf{\Phi}\mathbf{v}(t). \tag{36}$$

Using Moore-Penrose conditions, it can be shown that $\mathbf{\Phi}$ is an orthogonal projector, fulfilling the following properties: (1) $\mathbf{\Phi}^2 = \mathbf{\Phi}$, (2) $\mathbf{\Phi}^{\intercal} = \mathbf{\Phi}$. Moreover, $\mathbf{v}(t)$ is an arbitrary vector facilitating not only wide choices for the exploration path $\mathbf{a}(t)$, but also reducing a cost function of choice as t varies. Given such a cost function $\mathcal{K}(\mathbf{a}(t)) \in \mathbb{R}_0^{+}$, select the free function vector as

$$\mathbf{v}(t) = -\frac{\partial \mathcal{K}(\mathbf{a}(t))}{\partial \mathbf{a}(t)}. \tag{37}$$

Then, using the chain rule and properties of the projector $\mathbf{\Phi}$, it can be shown that

$$\frac{d\mathcal{K}(\mathbf{a}(t))}{dt} = -\left(\mathbf{\Phi}\frac{\partial \mathcal{K}(\mathbf{a}(t))}{\partial \mathbf{a}(t)}\right)^{\intercal}\left(\mathbf{\Phi}\frac{\partial \mathcal{K}(\mathbf{a}(t))}{\partial \mathbf{a}(t)}\right) \le 0. \tag{38}$$

According to (38), the cost function $\mathcal{K}(\mathbf{a}(t))$ is monotonically reduced as t grows. Moreover, if the cost function is chosen to have a quadratic form, such as

$$\mathcal{K}(\mathbf{a}(t)) = \frac{1}{2}\mathbf{a}^{\intercal}(t)\mathbf{D}\mathbf{a}(t), \tag{39}$$

where $\mathbf{D}$ is an $L_{N,m} \times L_{N,m}$ real-valued, symmetric, non-negative definite matrix, then the coefficients $a_i(t)$, $i = 1, \ldots, L_{N,m}$, will shrink under D-MORPH at rates depending on the elements of $\mathbf{D}$. More specifically, if $\mathbf{D}$ is a diagonal matrix, then relatively larger values may be assigned to appropriate diagonal entries to suppress contributions from high-order basis functions of GPCE. Combining (36), (37), and (39) yields an initial-value problem governed by the differential equation

$$\frac{d\mathbf{a}(t)}{dt} = -\mathbf{\Phi}\mathbf{D}\mathbf{a}(t), \ \mathbf{a}(0) = \mathbf{A}^{+}\mathbf{b}. \tag{40}$$

An analytically derived transient solution of (40) is

$$\mathbf{a}(t) = \exp(-t\mathbf{\Phi}\mathbf{D})\mathbf{a}(0) = \exp(-t\mathbf{\Phi}\mathbf{D})\mathbf{A}^{+}\mathbf{b},$$

paving the way for the steady-state or stationary solution to describe the final D-MORPH solution of the expansion coefficients. Indeed, by taking the limit $t \to \infty$ and invoking decomposition of $\mathbf{\Phi}\mathbf{D}$, the final D-MORPH solution is [23]

$$\bar{\mathbf{c}} = \lim_{t\to\infty}\mathbf{a}(t) = \mathbf{E}_{L_{N,m}-r}(\mathbf{F}_{L_{N,m}-r}^{\intercal}\mathbf{E}_{L_{N,m}-r})^{-1}\mathbf{F}_{L_{N,m}-r}^{\intercal}\,\mathbf{A}^{+}\mathbf{b},$$

where $\bar{\mathbf{c}} = (\bar{C}_1, \ldots, \bar{C}_{L_{N,m}})^{\intercal}$ with $\bar{C}_i \in \mathbb{R}$, $i = 1, \ldots, L_{N,m}$, representing the approximate coefficients of GPCE by the original D-MORPH regression and matrices $\mathbf{E}_{L_{N,m}-r}$ and $\mathbf{F}_{L_{N,m}-r}$ are constructed from the last $L_{N,m} - r$ columns of matrices $\mathbf{E}$ and $\mathbf{F}$ generated from the singular value decomposition of

$$\mathbf{\Phi}\mathbf{D} = \mathbf{E}\begin{bmatrix}\mathbf{T}_r & \mathbf{0}\\ \mathbf{0} & \mathbf{0}\end{bmatrix}\mathbf{F}^{\intercal}, \tag{41}$$

with $\mathbf{T}_r$ representing an $r \times r$ diagonal matrix comprising nonzero entries. The D-MORPH solution is unique and represents a linear combination of the elements of the initial solution $\mathbf{A}^{+}\mathbf{b}$.

6.3.2. Partitioned D-MORPH

The partitioned D-MORPH regression is new and applicable to either an underdetermined or an overdetermined system. This is accomplished by proposed segmented basis functions where the original regression problem is transformed into one with an underdetermined system.

For an arbitrary linear regression problem, whether $L < L_{N,m}$ or $L > L_{N,m}$, consider dividing the GPCE basis functions into two groups: (1) a primary group consisting of $L_p \leq L_{N,m}$ basis functions and (2) a secondary group comprising the remaining $L_{N,m} - L_p$ basis functions. The choice of which basis functions belong to the primary group or the secondary group depends on the problem at hand. However, a natural choice is to group them according to their relative importance. For instance, in many real-life problems, the low-order basis functions of GPCE contribute to a function value more significantly than the high-order basis functions of GPCE. In such a case, the low-order basis functions form the primary group, while the rest are lumped into the secondary group. In addition, the number of primary basis functions L_p should also depend on and preferably be less than the data size L. This is because a relatively small value of L will not provide accurate estimates of the expansion coefficients if L_p is decided based on $L_{N,m}$ alone. Indeed, when $L_p \leq L$, a D-MORPH solution ensures adequate accuracy in the primary group of coefficients while the secondary group of coefficients becomes nearly equal to zeros. Based on these considerations, the number of primary basis functions is defined as

$$L_p := \min\left(\left\lceil \frac{L_{N,m}}{K_1} \right\rceil, \left\lceil \frac{L}{K_2} \right\rceil\right), \tag{42}$$

where $K_1, K_2 \geq 1$ are two real-valued factors such that $L_p < L_{N,m}$ and $L_p < L$. Here, $\lceil \cdot \rceil$ is a symbol for the ceiling function. Again, the proper values of K_1, K_2 are problem dependent, meaning that there are no universal formulae for K_1 and K_2.

According to (42), there are two cases of how L_p is determined: (1) $L_p = \lceil L_{N,m}/K_1 \rceil$ and (2) $L_p = \lceil L/K_2 \rceil$. In this work, two different approaches have been proposed to deal with these two cases. In the first case, a straightforward version of the partitioned D-MORPH, called the direct approach, is utilized. In the second case, an iterated variant of the partitioned D-MORPH, referred to as the extended approach, is employed. Algorithm 1 explains the conditions for these two approaches.

Algorithm 1 Direct and extended approaches for the partitioned D-MORPH.

Input : K_1, K_2, L, $L_{N,m}$.
Set L_p according to (42).
If $L_p = \lceil L_{N,m}/K_1 \rceil$, use the direct approach.
If $L_p = \lceil L/K_2 \rceil$, use the extended approach.

Direct approach. Given $L_p < L_{N,m}$, consider partitioning the $L \times L_{N,m}$ matrix

$$\mathbf{A} = \begin{bmatrix} \mathbf{A}_p & \mathbf{A}_s \end{bmatrix}$$

into two parts, where $\mathbf{A}_p$ is the $L \times L_p$ matrix representing the first L_p columns of $\mathbf{A}$ and $\mathbf{A}_s$ is the $L \times (L_{N,m} - L_p)$ matrix describing the last $L_{N,m} - L_p$ columns of $\mathbf{A}$. Then the linear system (32) can be written as

$$\begin{bmatrix} \mathbf{A}_p^\intercal \\ \mathbf{A}_s^\intercal \end{bmatrix} \begin{bmatrix} \mathbf{A}_p & \mathbf{A}_s \end{bmatrix} \hat{\mathbf{c}} = \begin{bmatrix} \mathbf{A}_p^\intercal \\ \mathbf{A}_s^\intercal \end{bmatrix} \mathbf{b}. \tag{43}$$

Both (32) and (43) represent the same $L_{N,m}$ linear equations in $L_{N,m}$ variables and are solvable by SLS only if $L > L_{N,m}$ and $\text{rank}(\mathbf{A}) = L_{N,m}$. However, here, the objective is to solve the problem for arbitrary values of L and $L_{N,m}$.

Now consider only the first L_p equations of (43), that is,

$$\mathbf{A}_p^\intercal \begin{bmatrix} \mathbf{A}_p & \mathbf{A}_s \end{bmatrix} \hat{\mathbf{c}} = \mathbf{A}_p^\intercal \mathbf{b}. \tag{44}$$

As $L_p < L_{N,m}$ in the direct approach, the linear system (44) is underdetermined and readily solved by the D-MORPH regression. In other words, it is possible to create an underdetermined system whether the original regression problem begins with an underdetermined or overdetermined system.

Let

$$\bar{\mathbf{A}} := \mathbf{A}_p^\intercal \begin{bmatrix} \mathbf{A}_p & \mathbf{A}_s \end{bmatrix}$$

be the reduced $L_p \times L_{N,m}$ matrix and

$$\bar{\mathbf{b}} := \mathbf{A}_p^\intercal \mathbf{b}.$$

the reduced L_p-dimensional vector. Then a more compact version of (44) reads

$$\bar{\mathbf{A}} \hat{\mathbf{c}} = \bar{\mathbf{b}}. \tag{45}$$

Compared with (29), (45) is an underdetermined system and is readily solvable by D-MORPH regression, as described in the previous subsection. Indeed, treating $\bar{\mathbf{A}}$ as $\mathbf{A}$ and $\bar{\mathbf{b}}$ as $\mathbf{b}$, the GPCE expansion coefficients by D-MORPH regression are determined as

$$\check{\mathbf{c}} = \bar{\mathbf{E}}_{L_{N,m}-r}(\bar{\mathbf{F}}^{\intercal}_{L_{N,m}-r}\bar{\mathbf{E}}_{L_{N,m}-r})^{-1}\bar{\mathbf{F}}^{\intercal}_{L_{N,m}-r}\,\bar{\mathbf{A}}^{+}\bar{\mathbf{b}}. \tag{46}$$

Here, $\check{\mathbf{c}} = (\check{C}_1, \ldots, \check{C}_{L_{N,m}})^{\intercal}$ with $\check{C}_i \in \mathbb{R},\ i = 1, \ldots, L_{N,m}$, representing the approximate coefficients of GPCE by the direct approach of the partitioned D-MORPH regression and $\bar{\mathbf{A}}^{+}$ is the Moore-Penrose inverse of $\bar{\mathbf{A}}$, $\bar{\mathbf{E}}_{L_{N,m}-r}$ and $\bar{\mathbf{F}}_{L_{N,m}-r}$ are constructed from the last $L_{N,m} - r$ columns of $\mathbf{E}$ and $\mathbf{F}$, generated from the singular value decomposition of

$$\bar{\mathbf{\Phi}}\bar{\mathbf{D}} = \bar{\mathbf{E}}\begin{bmatrix}\bar{\mathbf{T}}_r & \mathbf{0}\\ \mathbf{0} & \mathbf{0}\end{bmatrix}\bar{\mathbf{F}}^{\intercal},$$

where

$$\bar{\mathbf{\Phi}} := (\mathbf{I}_{L_{N,m}} - \bar{\mathbf{A}}^{+}\bar{\mathbf{A}}) \in \mathbb{R}^{L_{N,m}\times L_{N,m}},$$

$$\bar{\mathbf{D}} = \mathrm{diag}[\underbrace{0, \cdots, 0}_{L_p}, \underbrace{1, \cdots, 1}_{L_{N,m}-L_p}],$$

and $\bar{\mathbf{T}}_r$ is an $r \times r$ diagonal matrix comprising non-zero entries. Here, the diagonal matrix $\bar{\mathbf{D}}$ comprises zeros and ones meant for the primary and secondary groups, respectively. The cost function with the first L_p-zeros setting in the weight values contributes to the shrinkage of the solution in the secondary group to nearly zeros. According to a D-MORPH property that preserves the data fitting, the given data set is fitted mostly to the primary basis functions. Thereby, under the $L_p < L$ condition, the primary part of direct partitioned D-MORPH solution should have accuracy close to the SLS solution for the overdetermined linear system: $\mathbf{A}_p\mathbf{c}_p = \mathbf{b}$, where $\mathbf{c}_p$ comprises estimates of L_p expansion coefficients. Indeed, if $L_p = \lceil L_{N,m}/K_1 \rceil$ is chosen and L is sufficiently large, then the partitioned D-MORPH with the direct approach is expected to furnish the best solution to the normal equation (45) for the estimated GPCE coefficients.

Extended approach. In the extended approach, the primary group is determined from $L_p = \lceil L/K_2 \rceil$, meaning that $L_p < L$. If, in addition, the data size L is small, then the primary group may be not large enough to represent an output value accurately, requiring better estimation of the GPCE coefficients in the secondary group. As will be seen later, by defining a new cost function, generated from the solution of the direct approach, an improved D-MORPH solution is possible. The final solution of the GPCE coefficients is denoted by $\mathbf{c}' \in \mathbb{R}^{L_{N,m}}$.

The construction of the new cost function involves two principal steps. First, the GPCE coefficients using the direct approach of the partitioned D-MORPH are estimated, obtaining $\check{\mathbf{c}} \in \mathbb{R}^{L_{N,m}}$ from (46). Second, using the coefficients from the direct approach, a revised solution $\mathbf{c}'_0 = (C'_{0,1}, \ldots, C'_{0,L_{N,m}})^{\intercal}$ of the GPCE coefficients is defined as

$$C'_{0,j} := \begin{cases}\check{C}_j, & j = 1, \ldots, L_p,\\ k_j, & j = L_p + 1, \ldots, L_{N,m},\end{cases} \tag{47}$$

where $\check{C}_j$ is the jth coefficient obtained from the direct approach of the partitioned D-MORPH solution $\check{\mathbf{c}}$ in the primary group and k_j is a revised estimate of the jth coefficient in the secondary group. According to (47), the primary coefficients are preserved from the direct solution, but the secondary coefficients undergo a revision by replacing them with k_j, which needs to be defined. While there is no universal formula for k_j, a possible way of expressing of k_j, used in this work, involves averaging a set of relevant coefficients from the primary group. In reference to (4), let

$$\mathcal{L}_k = \left\{j \ :\ \left|\mathbf{j}^{(j)}\right| = \left|\mathbf{j}^{(k)}\right|,\ j = 1, \ldots, k\right\},\ k = 1, \ldots, L_{N,m}, \tag{48}$$

be a set of subscript j for the jth polynomial function of the same degree as $\Psi_{\mathbf{j}^{(k)}}$. Then, one way to set $\mathbf{c}'_0$ in the secondary group for GPCE is by

$$k_j = \begin{cases}\left|\dfrac{1}{\#\mathcal{L}_{j-1}}\displaystyle\sum_{l\in\mathcal{L}_{j-1}}\check{C}_l\right|, & j = L_p+1,\ \left|\mathbf{j}^{(j)}\right| = \left|\mathbf{j}^{(L_p)}\right|,\\ \beta\left|\dfrac{1}{\#\mathcal{L}_{j-1}}\displaystyle\sum_{l\in\mathcal{L}_{j-1}}\check{C}_l\right|, & j = L_p+1,\ \left|\mathbf{j}^{(j)}\right| > \left|\mathbf{j}^{(L_p)}\right|,\\ k_{j-1}, & j > L_p+1,\ \left|\mathbf{j}^{(j)}\right| = \left|\mathbf{j}^{(j-1)}\right|,\\ \beta k_{j-1}, & j > L_p+1,\ \left|\mathbf{j}^{(j)}\right| > \left|\mathbf{j}^{(j-1)}\right|,\end{cases} \tag{49}$$

where $\check{C}_l$ is the lth element of the direct approach of the partitioned D-MORPH solution $\check{\mathbf{c}}$, and $\beta \in (0, 1]$; this may be set differently depending on the problem, but here it has a default value of 0.5. In (49), the same symbol $|\cdot|$ is used to denote the degree of $\mathbf{j}$ multi-index and the absolute value of a function. Here, (49) is motivated by the desire that the

Table 1
Degree-wise arranged expansion coefficients ($N = 2,\ m = 3$).

$\lvert\mathbf{j}^{(j)}\rvert = 0$	$\lvert\mathbf{j}^{(j)}\rvert = 1$	$\lvert\mathbf{j}^{(j)}\rvert = 2$	$\lvert\mathbf{j}^{(j)}\rvert = 3$
$\check{C}_1$	$\check{C}_2$	$\check{C}_4$	$\check{C}_7$
	$\check{C}_3$	$\check{C}_5$	$\check{C}_8$
		$\check{C}_6$	$\check{C}_9$
			$\check{C}_{10}$

corresponding coefficients of the basis functions of the same degree $|\mathbf{j}^{(j)}|$ decrease with the ratio β to the degree $|\mathbf{j}^{(j)}| - 1$. As an example, consider a special case where $N = 2,\ m = 3,\ L_{N,m} = 10$, and $L_p = 5$. In this case, the solution of GPCE coefficients from the direct approach is a ten-dimensional vector $(\check{C}_1, \ldots, \check{C}_{10})^\intercal$, and its elements can be grouped in the corresponding degree $|\mathbf{j}^{(j)}|$ in Table 1. Thereafter, the fifth element of the solution is $\check{C}_5$ and the corresponding degree $|\mathbf{j}^{(5)}|$ is 2. Then, from (48), $\mathcal{L}_5 = \{4, 5\}$ and $\#\mathcal{L}_5 = 2$. According to (49), the secondary group of GPCE coefficients are obtained as follows:

$$k_j = \begin{cases} \left|\dfrac{\check{C}_4 + \check{C}_5}{2}\right|, & j = 6, \\ \beta k_6, & j = 7, \\ k_7, & j = 8, 9, 10. \end{cases}$$

Once the revised solution is formulated, define the new cost function

$$\mathcal{K}'(\mathbf{a}(t)) = \frac{1}{2}\left[\sum_{i=1}^{L_{N,m}} (a_i(t) - C'_{0,i})^2\right] = \frac{1}{2}(\mathbf{a}(t) - \mathbf{c}'_0)^\intercal(\mathbf{a}(t) - \mathbf{c}'_0). \tag{50}$$

By combining (36), (37), and (50), an initial-value problem for ordinary differential equation is now derived as

$$\frac{d\mathbf{a}(t)}{dt} = -\bar{\mathbf{\Phi}}(\mathbf{a}(t) - \mathbf{c}'_0),\ \mathbf{a}(0) = \bar{\mathbf{A}}^+\bar{\mathbf{b}}. \tag{51}$$

Note that (51) is nonhomogeneous with the transient solution

$$\mathbf{a}(t) = \exp(-t\bar{\mathbf{\Phi}})\bar{\mathbf{A}}^+\bar{\mathbf{b}} + \int_0^t \exp\{-(t-s)\bar{\mathbf{\Phi}}\}\bar{\mathbf{\Phi}}\mathbf{c}'_0 ds, \tag{52}$$

where a particular solution is included on the second term of right-hand side of (52). Finally, by taking the limit $t \to \infty$, the unique partitioned D-MORPH solution is

$$\mathbf{c}' = \bar{\mathbf{E}}'_{L_{N,m}-r}(\bar{\mathbf{F}}'^\intercal_{L_{N,m}-r}\bar{\mathbf{E}}'_{L_{N,m}-r})^{-1}\bar{\mathbf{F}}'^\intercal_{L_{N,m}-r}\ \bar{\mathbf{A}}^+\bar{\mathbf{b}} + \bar{\mathbf{E}}'_r(\bar{\mathbf{F}}'^\intercal_r\bar{\mathbf{E}}'_r)^{-1}\bar{\mathbf{F}}'^\intercal_r\bar{\mathbf{T}}'^{-1}_r\ \bar{\mathbf{\Phi}}\mathbf{c}'_0,$$

where $\mathbf{c}' = (C'_1, \ldots, C'_{L_{N,m}})^\intercal$ with $C'_i \in \mathbb{R},\ i = 1, \ldots, L_{N,m}$, representing the approximate coefficients of GPCE by the extended approach of the partitioned D-MORPH regression and $\bar{\mathbf{E}}'_r$ and $\bar{\mathbf{E}}'_{L_{N,m}-r}$, $\bar{\mathbf{F}}'_r$ and $\bar{\mathbf{F}}'_{L_{N,m}-r}$ are constructed from the first r and the last $L_{N,m} - r$ columns of matrices respectively $\bar{\mathbf{E}}'$ and $\bar{\mathbf{F}}'$, generated from the singular value decomposition of $\bar{\mathbf{\Phi}}$ as

$$\bar{\mathbf{\Phi}} = \bar{\mathbf{E}}'\begin{bmatrix}\bar{\mathbf{T}}'_r & \mathbf{0} \\ \mathbf{0} & \mathbf{0}\end{bmatrix}\bar{\mathbf{F}}'^\intercal,$$

with $\bar{\mathbf{T}}'_r$ representing an $r \times r$ diagonal matrix including nonzero entries.

The solution $\mathbf{c}'$ from the extended approach is a linear combination of the initial solution $\bar{\mathbf{A}}^+\bar{\mathbf{b}}$ and the direct partitioned D-MORPH solution with revised estimates of the secondary group $\mathbf{c}'_0$.

Li and Rabitz, in a subsequent work, [26] described D-MORPH regression for overdetermined systems. Their method is similar to the partitioned D-MORPH regression in the sense that it involves two classes of basis functions. However, instead of partitioning current basis functions, as done here, they opted to augment the linear system by supplementing new basis functions to the pool of existing ones. While such augmentations may be useful in some applications, doing so in the context of GPCE is not recommended for several reasons. First, the proliferation of GPCE basis functions is exponential with respect to the order m. Therefore, for large N, increasing the order m even by *one* will lead to numerous additional basis functions and significant escalation of the computational cost. Second, for new basis functions, the monomial moment matrix has to be reconstructed, followed by whitening transformation to generate the corresponding vector of orthonormal polynomials. Third, the additional basis may not be necessary for improving the quality of the GPCE approximation. In contrast, the proposed partitioning approach focuses on accurate calculation of the low-order expansion coefficients while shrinking, as much as possible, the high-order expansion coefficients, thereby reducing the effect of overfitting while maintaining approximation quality.

It is important to underscore that, for UQ analysis under dependent random variables, the application of SLS and D-MORPH regression for estimating the GPCE coefficients is novel. Existing related works on regression are limited to classical PCE mandating tensor-product structure [24]. In contrast, no tensor-product structure is required or enforced in this work. More importantly, the proposed partitioned D-MORPH is a new variant of regression method that should be useful not only in the context of GPCE, as demonstrated here, but also in solving general high-dimensional regression problems.

7. Practical GPCE approximation

The mth-order GPCE approximation presented in Section 4 is idealistic. This is because neither the orthonormal polynomials nor the expansion coefficients are exactly calculable for a general UQ problem subject to an arbitrary output function and arbitrary probability distribution of input random variables. In this section, a workable GPCE approximation, relevant to solving practical UQ problems, is emphasized.

7.1. Implementable GPCE approximation

Due to the construction of the monomial moment matrix from numerical integration or sampling methods, the resulting whitening matrix, as described in Section 5, is determined approximately. Therefore, the actual, approximate orthonormal polynomials are $\tilde{\Psi}_i(\mathbf{x})$, $i = 1, \ldots, L_{N,m}$. In addition, using the regression methods presented in Section 6, the expansion coefficients are $\tilde{C}_i$, $i = 1, \ldots, L_{N,m}$, also approximate. Therefore, instead of (14), an actual mth-order GPCE approximation of $y(\mathbf{X})$ is

$$\tilde{y}_m(\mathbf{X}) = \sum_{i=1}^{L_{N,m}} \tilde{C}_i \tilde{\Psi}_i(\mathbf{X}),$$

which is ready to be implemented for a general UQ problem. Given a desired regression method described in Section 6, there exist four distinct estimates of $\tilde{C}_i$: (1) $\hat{C}_i$ by the SLS regression; (2) $\bar{C}_i$ by the original D-MORPH regression; (3) $\check{C}_i$ by the direct approach of the partitioned D-MORPH regression; and (4) C'_i by the extended approach of the partitioned D-MORPH regression. Three of these estimates will be used in numerical examples.

Thenceforth, the mean and variances of $\tilde{y}_m(\mathbf{X})$ are calculated from the estimated expansion coefficients as

$$\mathbb{E}[\tilde{y}_m(\mathbf{X})] \approx \tilde{C}_1 \tag{53}$$

and

$$\mathrm{var}[\tilde{y}_m(\mathbf{X})] \approx \sum_{i=2}^{L_{N,m}} \tilde{C}_i^2, \tag{54}$$

respectively.

Similarly, for reliability analysis, the approximate failure probability is determined from

$$\tilde{P}_{F,m} = \mathbb{E}\left[I_{\tilde{\Omega}_{F,m}}(\mathbf{X})\right] = \lim_{L' \to \infty} \frac{1}{L'} \sum_{l=1}^{L'} I_{\tilde{\Omega}_{F,m}}(\mathbf{x}^{(l)}), \tag{55}$$

where $\tilde{\Omega}_{F,m} := \{\mathbf{x} : \tilde{y}_m(\mathbf{x}) < 0\}$ is the approximate failure set as a result of an mth-order actual GPCE approximation $\tilde{y}_m(\mathbf{X})$. All numerical results of second-moment statistics and reliability analysis reported in the paper are based on the actual GPCE approximation and formulae described in (53), (54), and (55).

7.2. Computational cost and flow

For expensive-to-run computational models, the cost for creating an mth-order GPCE approximation stems mostly from the construction of the experimental design, resulting in the input-output data set $\{\mathbf{x}^{(l)}, y(\mathbf{x}^{(l)})\}_{l=1}^{L}$ of size $L \in \mathbb{N}$. When the effort in calculating the output function is independent of the input data — the case commonly dealt with in modeling and simulation of mechanical systems — then the computational cost is directly proportional to the data size L. For SLS regression, L is several times larger than $L_{N,m}$. Since the number of GPCE basis functions or expansion coefficients grows rapidly with respect to both N and m, minimizing L relative to $L_{N,m}$ is a fundamental practical requirement. In this regard, the proposed partitioned D-MORPH regression method is envisioned to markedly accelerate the application of GPCE for solving realistic UQ problems.

Fig. 1 presents a general computational flow for constructing a practical GPCE approximation. It includes calculation of the second-moment properties and reliability of a complex mechanical system.

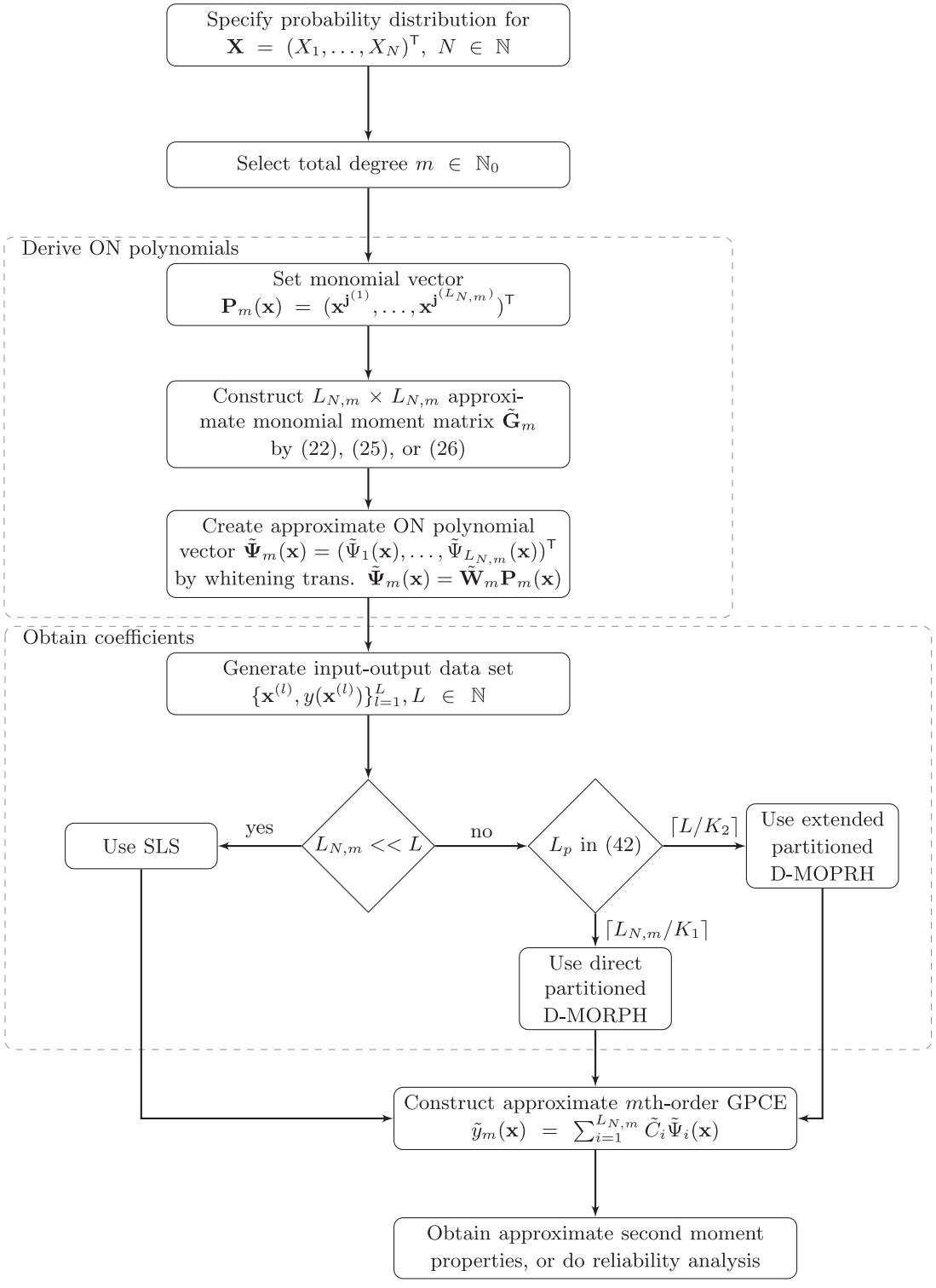

Fig. 1. A computation flow for generating a practical GPCE approximation.

8. Numerical examples

Four numerical examples, each following a specific objective, are presented to illustrate UQ analysis by GPCE under dependent random variables. While Example 1 determines the approximation quality of measure-consistent orthonormal polynomials, Examples 2–4 entail statistical moment and reliability analyses, which are the focus of this work.

The approximate orthonormal polynomials in Example 1 were generated using both numerical integration and QMCS for constructing the monomial moment matrix. For the numerical integration, Option 1 with an isotropic Gauss quadrature rule was selected, where the transformed variables follow independent standard Gaussian distributions for the unbounded rectangular domain ($\mathbb{A}^2 = \mathbb{R}^2$) and independent uniform distributions over [0,1] for the bounded non-rectangular domains ($\mathbb{A}^2 = \mathbb{B}^2$ or $\mathbb{T}^2$). The orders (n) of the Gauss quadrature rule are 15, 20, and 100 for the Gaussian, Gegenbauer, and Dirichlet distributions of $\mathbf{X}$, respectively, which was determined from convergence tests. The sample size (L'') of QMCS, performed in conjunction with the Sobol sequence, is 5×10^5 for all three probability measures of Example 1.

In Examples 2–4, Option 2 with an isotropic Gauss quadrature was employed to construct the monomial moment matrix solely by numerical integration. The order of integration varies as 16 (Case 1), 57 (Case 2), 33 (Case 3) in Example 2, whereas the orders are 7 in Example 3, and 10 in Example 4. When calculating the failure probability or distribution function in Examples 2–4, the sample size (L') of resampling is 10^6. In the three latter examples, standard MCS was employed to construct the input-output data set. For the partitioned D-MORPH, the number of basis functions in the primary group L_p is determined by $\min(\lceil L_{N,m}/2.5 \rceil, \lceil L/2 \rceil)$ in Example 3 and $\min(\lceil L_{N,m}/2.1 \rceil, \lceil L/6 \rceil)$ in Example 4. The default value of β for the extended approach of the partitioned D-MORPH is 0.5 in both Examples 3 and 4. The sample sizes (L_{MCS}) for standard MCS used to evaluate the accuracy of GPCE solutions are 10^6 in Examples 2 and 3, and 3000 in Example 4. Finally, the relative error used in Example 2 is defined as the absolute value of the ratio of the difference between approximate and benchmark solutions and benchmark solution. The benchmark solution is either an exact solution, or the solution from standard MCS or numerical integration.

8.1. Example 1: multivariate orthonormal polynomials

The first example delves into generation of measure-consistent orthonormal polynomials in two variables. Three distinct cases of the probability density functions of random variables X_1 and X_2 are selected as follows.

(1) A Gaussian density on $\mathbb{R}^2$:

$$f_{X_1X_2}(x_1, x_2) = \frac{1}{2\pi\sigma_1\sigma_2\sqrt{1-\rho^2}} \exp\left[-\frac{1}{2(1-\rho^2)}\left(\frac{x_1^2}{\sigma_1^2} - \frac{2\rho x_1 x_2}{\sigma_1\sigma_2} + \frac{x_2^2}{\sigma_2^2}\right)\right], \quad -\infty < x_1, x_2 < +\infty.$$

(2) A Gegenbauer density on the unit disk $\mathbb{B}^2$:

$$f_{X_1X_2}(x_1, x_2) = \begin{cases} \frac{1}{\pi}\left(\mu + \frac{1}{2}\right)(1 - x_1^2 - x_2^2)^{\mu - \frac{1}{2}}, & 0 \le x_1^2 + x_2^2 \le 1, \\ 0, & \text{otherwise.} \end{cases}$$

(3) A Dirichlet density on the standard triangle $\mathbb{T}^2$:

$$f_{X_1X_2}(x_1, x_2) = \begin{cases} \frac{\Gamma(\lambda_1 + \lambda_2 + \lambda_3 + 3) x_1^{\lambda_1} x_2^{\lambda_2} (1 - x_1 - x_2)^{\lambda_3}}{\Gamma(\lambda_1 + 1)\Gamma(\lambda_2 + 1)\Gamma(\lambda_3 + 1)}, & 0 \le x_1, x_2; x_1 + x_2 \le 1, \\ 0, & \text{otherwise.} \end{cases}$$

Fig. 2 plots all three density functions for the following choices of the parameters: $\sigma_1 = \sigma_2 = 1/4$, $\rho = 2/5$, $\mu = 4$, and $\lambda_1 = \lambda_2 = \lambda_3 = 3$.

A primary motivation for picking Gaussian, Gegenbauer, and Dirichlet density functions emerges from the fact that all three densities are endowed with a Rodrigues-type formula. As a result, measure-consistent orthonormal polynomials can be generated exactly [12]. Table A.1 from Appendix A shows such polynomials of degree at most three ($m = 3$) for the chosen values of the density parameters. The objective of this example is to draw on these exact orthonormal polynomials to establish the accuracy of the proposed three-step algorithm in producing approximate orthonormal polynomials.

As described in Sections 5.1.1 and 5.1.2, both isotropic Gauss quadrature (numerical integration) and QMCS (sampling method) were employed to assemble the monomial moment matrix $\tilde{\mathbf{G}}_3$ for each of the three aforementioned density functions. Tables A.2 and A.3 from Appendix A list the desired measure-consistent orthonormal polynomials from the three-step algorithm when the monomial matrix is estimated by numerical integration and a sampling method, respectively. A comparison between the approximate polynomials $\tilde{\boldsymbol{\Psi}}_3(x_1, x_2)$ in Table A.2 and their exact counterparts $\boldsymbol{\Psi}_3(x_1, x_2)$ in Table A.1 confirm very high accuracy of the three-step algorithm, especially when numerical integration is employed to construct $\tilde{\mathbf{G}}_3$. The approximation quality of polynomials in Table A.3 is also very good for the sample size of QMCS chosen. The performance of QMCS should improve if the sample size L'' increases. While QMCS does not appear to bring any tangible benefit in this example entailing only two variables, it may become competitive in high-dimensional applications where numerical integration may not be feasible. Nonetheless, these results provide confidence in generating orthonormal polynomials for other probability measures considered in the three remaining examples.

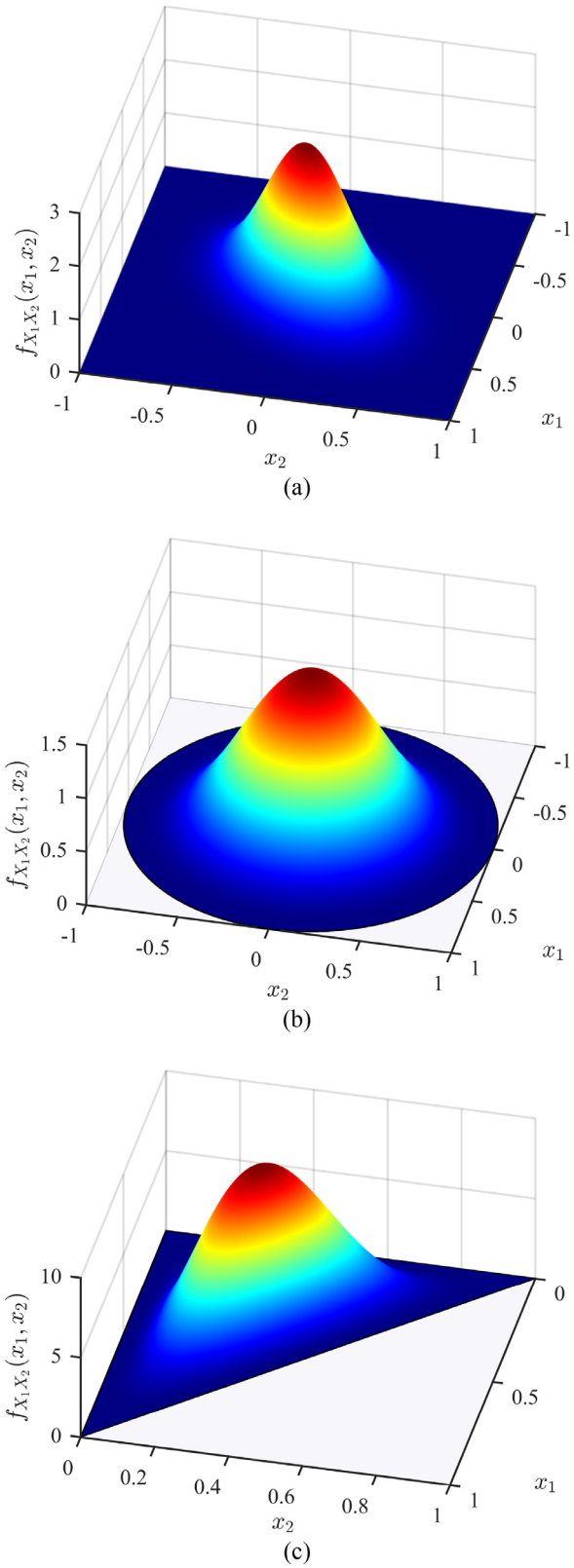

Fig. 2. Joint probability density functions of input random variables (Example 1); (a) a Gaussian density on $\mathbb{R}^2$; (b) a Gegenbauer density on the unit disk $\mathbb{B}^2$; (c) a Dirichlet density on the standard triangle $\mathbb{T}^2$.

8.2. Example 2: three mathematical functions

The objective of the second example is to establish the credibility of GPCE solutions for elementary mathematical functions when the expansion coefficients are estimated by the SLS regression. While there is nothing fundamentally new in the SLS regression by itself, the application of SLS regression to the calculation of GPCE coefficients is novel. In this regard, three distinct cases of polynomial output functions in two input random variables X_1 and X_2, each with its own unique density function defined by exponential, extreme-value, and lognormal distributions, were studied. They are described as follows:

(1) A linear polynomial and exponential distribution

$$y(X_1, X_2) = 18 - 3X_1 - 2X_2,$$

$$f_{X_1X_2}(x_1, x_2) = \begin{cases} \exp[-(x_1 + x_2 + x_1x_2)][(1 + x_1)(1 + x_2) - 1], & 0 \le x_1, x_2 < \infty, \\ 0, & \text{otherwise.} \end{cases}$$

(2) A quadratic polynomial and extreme-value distribution

$$y(X_1, X_2) = 49 - X_1^2 - X_2^2,$$

$$\begin{aligned} f_{X_1X_2}(x_1, x_2) = {} & \exp\left[-\exp(-x_1) - \exp(-x_2) + \frac{1}{\exp(x_1) + \exp(x_2)}\right] \times \exp(-x_1 - x_2) \\ & \times \left[1 - \left(\frac{\exp(2x_1) + \exp(2x_2)}{\{\exp(x_1) + \exp(x_2)\}^2} + 2\frac{\exp(2x_1) + \exp(2x_2)}{\{\exp(x_1) + \exp(x_2)\}^3} + \frac{\exp(2x_1) + \exp(2x_2)}{\{\exp(x_1) + \exp(x_2)\}^4}\right)\right], \\ & -\infty < x_1, x_2 < \infty. \end{aligned}$$

(3) A quartic polynomial and lognormal-normal distribution

$$y(X_1, X_2) = 2500 - \frac{1}{2}(4X_1 - 5X_2^2)^2,$$

$$f_{X_1X_2}(x_1, x_2) = \begin{cases} \dfrac{50}{3\sqrt{19}\pi x_1} \exp\left[-\dfrac{50}{19}\left\{\left(\dfrac{10\ln x_1 - 20}{3}\right)^2 + (x_2 - 1)^2 + \dfrac{9}{5}\left(\dfrac{10\ln x_1 - 20}{3}\right)(x_2 - 1)\right\}\right], & 0 \le x_1 < \infty; -\infty < x_2 < \infty \\ 0, & \text{otherwise.} \end{cases}$$

Depending on the output function, the order of GPCE approximations varies as follows: $m = 1$ in Case 1, $m = 2$ in Case 2, and $m = 4$ in Case 3. Correspondingly, the number of basis functions or expansion coefficients are 3, 6, and 15, respectively. The factor $L/L_{N,m}$ involved in the SLS regression changes from 1 to 4, which was decided by trial and error. For the benchmark solutions in Cases 1, 2, and 3, the mean values are 13, 45.03120, and 2089.03370, respectively, and the standard deviation values are 2.85594, 8.22874, and 378.68671, respectively.

8.2.1. Statistical moment analysis

Table 2 presents relative errors in the mean and standard deviation of $y(X_1, X_2)$ committed by the respective GPCE approximations for all three cases. The corresponding numbers of function evaluations, which are the same as the data size L, are tabulated in the last column. Although the output functions here are all polynomials, the GPCE errors do not vanish as the expansion coefficients and orthonormal polynomials are both calculated approximately. Nonetheless, they are negligibly small, given how small the data size is. To judge the computational efficacy of GPCE, the errors perpetrated by the classical tensor-product PCE, valid strictly for independent random variables, were also determined. This was managed by a Rosenblatt transformation, where the dependent random variables are mapped to independent Gaussian variables, resulting in highly nonlinear non-polynomial functions. The coefficients of classical PCE were calculated by numerical integration, giving the best possible comparison to the GPCE estimates. Also, the integration orders in Cases 1, 2, and 3 are $2(m+1)$, $2(m+1)$, and $m+1$, respectively, fulfilling convergence. To achieve the same order of error of GPCE, a 7th- or 8th-order PCE approximation, depending on the function, is necessary in some cases. Correspondingly, the requisite number of function evaluations from the classical PCE increases by an order of magnitude. Therefore, by dealing with dependent variables head on, GPCE not only avoids the need for a very high-order PCE approximation, but also delivers satisfactory estimates of the second-moment properties of $y(X_1, X_2)$ while sustaining low computational cost.

8.2.2. Reliability analysis

Table 3 lists the failure probability estimates associated with all three output functions by GPCE approximations and standard MCS or exact solution. Compared with the exact or MCS-generated results, the failure probabilities calculated by GPCE approximations are quite accurate. For an additional comparison, a classical reliability method, such as the first-order reliability method (FORM), was employed to obtain associated approximations of the failure probability. Unfortunately, the results

Table 2
Relative errors in the second-moment properties of three functions by GPCE and PCE methods (Example 2).

	Relative error[a]		No. of function evaluations[b]
	Mean	Standard deviation	
(1) A linear polynomial and exponential distribution			
1st-order GPCE	1.4×10^{-15}	1.5×10^{-5}	3
5th-order PCE	1.3×10^{-6}	2.0×10^{-4}	144
6th-order PCE	4.8×10^{-7}	5.6×10^{-5}	196
7th-order PCE	1.5×10^{-7}	3.7×10^{-5}	256
(2) A quadratic polynomial and extreme value distribution			
2nd-order GPCE	2.7×10^{-4}	3.6×10^{-4}	6
6th-order PCE	2.8×10^{-4}	1.0×10^{-3}	196
7th-order PCE	2.8×10^{-4}	9.9×10^{-4}	256
8th-order PCE	2.8×10^{-4}	9.9×10^{-4}	324
(3) A quartic polynomial and lognormal-normal distribution			
4th-order GPCE	4.5×10^{-8}	1.8×10^{-7}	15
4th-order PCE	4.4×10^{-8}	1.9×10^{-6}	25
5th-order PCE	9.7×10^{-9}	2.0×10^{-6}	36
6th-order PCE	9.0×10^{-9}	3.5×10^{-7}	49

[a] The benchmark solution of (1) is exact; (2) and (3) are estimated by standard MCS and numerical integration.
[b] The total number of times the original response function is calculated.

Table 3
Failure probabilities associated with three performance functions calculated by GPCE and other methods (Example 2).

Method	Failure probability	No. of function evaluations[b]
	$\mathbb{P}[y(\mathbf{X}) < 0]$[a]	
(1) A linear polynomial and exponential distribution		
1st-order GPCE[c]	3.02×10^{-3}	3
Standard MCS	3.02×10^{-3}	1,000,000
FORM		
Transformation 1[d]		
1st MPP	2.70×10^{-3}	35[e]
2nd MPP	2.32×10^{-4}	
Transformation 2[f]		
1st MPP	4.00×10^{-3}	45[e]
2nd MPP	1.40×10^{-4}	
Exact	2.95×10^{-3}	
(2) A quadratic polynomial and extreme value distribution		
2nd-order GPCE[c]	6.00×10^{-3}	6
Standard MCS	6.00×10^{-3}	1,000,000
FORM		
1st MPP	5.50×10^{-3}	43[e]
2nd MPP	0	
(3) A quartic polynomial and lognormal-normal distribution		
4th-order GPCE[c]	1.10×10^{-3}	15
Standard MCS	1.10×10^{-3}	1,000,000
FORM		
1st MPP	1.52×10^{-4}	42[e]
2nd MPP	1.00×10^{-3}	

[a] (1) $y(\mathbf{X}) = 18 - 3X_1 - 2X_2$; (2) $y(\mathbf{X}) = 49 - X_1^2 - X_2^2$; (3) $y(\mathbf{X}) = 2500 - \frac{1}{2}(4X_1 - 5X_2^2)^2$.
[b] The total number of times the original response function is calculated.
[c] GPCE approximation is embedded with MCS (10^6).
[d] $T_1 \equiv (x_1, x_2) \rightarrow (u_1, u_2)$ on standard Gaussian space.
[e] The sum of 1st MPP and 2nd MPP in the number of function evaluations.
[f] $T_2 \equiv (x_2, x_1) \rightarrow (u_1, u_2)$ on standard Gaussian space.

of FORM are rather complicated due to the existence of multiple most probable points (MPPs) and non-uniqueness of the Rosenblatt transformation. In consequence, additional calculations are required to derive all possible solutions. Table 3 compiles multiple results of FORM, some of which are fairly accurate, but not all. More importantly, in the absence of MCS or other benchmark solutions, it is difficult to know which failure probability estimate by FORM is a credible one. No such problems are encountered in GPCE. It is interesting to note that FORM, which is known for its computational proficiency, is still more expensive than GPCE, at least in this example.

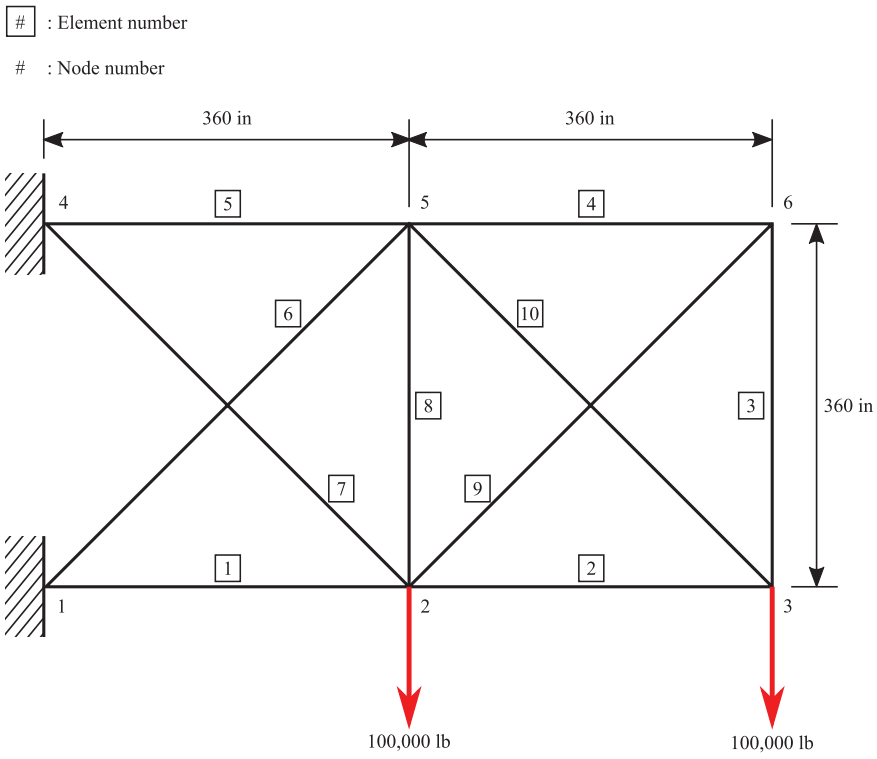

Fig. 3. A ten-bar truss structure (Example 3).

8.3. Example 3: a ten-bar truss

In the third example, a linear-elastic ten-bar truss was analyzed to determine the accuracy and computational efficiency of GPCE in component reliability analysis. As shown in Fig. 3, the truss is simply supported at nodes 1 and 4 and is subjected to two vertically downward concentrated forces of 100,000 lb at nodes 2 and 3. The material is aluminum alloy, which has Young's modulus of 10^7 psi. There are ten ($N = 10$) random variables $\mathbf{X} = (X_1, \ldots, X_{10})^\intercal$, representing random cross-sectional areas of all ten bars. Modeled as correlated lognormal random variables, they have identical means $\mu_i := \mathbb{E}[X_i] = 30$ in^2, standard deviations $\sigma_i = 4.5\,\text{in}^2$, and correlation coefficients $\rho_{ij} = 0.3973$, $i, j = 1, \ldots, 10$, $i \neq j$. According to a linear-elastic FEA, the maximum vertical displacement $v_3(\mathbf{X})$ occurs at node 3, where the permissible displacement is limited to 1.7 in. The analysis also reveals that the maximum axial stress $\sigma_1(\mathbf{X})$ occurs in bar 1, where the allowable stress is fixed at 10,800 psi. Thereby, two performance functions,

$$y_1(\mathbf{X}) := 1.7 - v_3(\mathbf{X}) \quad \text{and} \quad y_2(\mathbf{X}) := 10,800 - \sigma_1(\mathbf{X}),$$

stemming, respectively, from the displacement- and stress-based design considerations, were considered to define two failure probabilities as follows:

$$P_{F,1} := \mathbb{P}[y_1(\mathbf{X}) < 0], \quad P_{F,2} := \mathbb{P}[y_2(\mathbf{X}) < 0].$$

The objective is to calculate these two failure probabilities by GPCE approximations in conjunction with both SLS and partitioned D-MORPH regression methods for obtaining the expansion coefficients.

Table 4 presents two failure probabilities of the truss structure, calculated using several GPCE approximations and standard MCS. The GPCE solutions from both the second-order ($m = 2$) and third-order ($m = 3$) approximations were examined, whereas SLS and/or partitioned D-MORPH regression methods with varying numbers of FEA or data size (L) were used to estimate the corresponding coefficients. Clearly, the smaller the value of L, the lower the requisite computational cost. Therefore, calculating the failure probabilities with a low value of L is desired. According to Table 4, the second-order GPCE solution, obtained using SLS regression and 150 FEA for either performance function, is inadequate, as the respective estimates of the failure probability are far from their MCS predictions. The third-order GPCE approximation is necessary, as it provides markedly better results than the second-order GPCE approximation, regardless of the regression method used.

All estimates from the third-order GPCE approximation are fairly close to the MCS results for both performance functions. Yet, the required number of FEA varies considerably. For instance, to obtain satisfactory results from the third-order GPCE approximation, the SLS regression requires 350 FEA. In coherence with the number of basis or coefficients $L_{10,3} = 286$, a larger value of $L = 350$ yields an overdetermined system, which is necessary for the SLS regression. The direct approach

Table 4
Two failure probabilities of the truss structure calculated by GPCE and other methods (Example 3).

Method	Failure probability $\mathbb{P}[y_1(\mathbf{X}) < 0]$[a]	Failure probability $\mathbb{P}[y_2(\mathbf{X}) < 0]$[b]	Number of FEA
2nd order GPCE			
SLS	9.58×10^{-3}	2.22×10^{-4}	150
3rd order GPCE			
SLS	1.11×10^{-2}	5.56×10^{-4}	350
Partitioned D-MORPH			
Extended approach[c]			
data size=50	1.08×10^{-2}	4.69×10^{-4}	50
data size=150	1.21×10^{-2}	5.40×10^{-4}	150
Direct approach[d]			
data size=350	1.08×10^{-2}	5.38×10^{-4}	350
Standard MCS	1.15×10^{-2}	7.22×10^{-4}	1,000,000

[a] $y_1(\mathbf{X}) = 1.7 - v_3(\mathbf{X})$.
[b] $y_2(\mathbf{X}) = 10,800 - \sigma_1(\mathbf{X})$.
[c] $L_p = \lceil L/K_2 \rceil$, so the extended approach is followed by the direct approach according to Algorithm 1.
[d] $L_p = \lceil L_{N,m}/K_1 \rceil$, so only the direct approach is used according to Algorithm 1.

Table 5
Statistical properties of input random variables for UQ analysis of the connecting rod (Example 4).

Mean vector $\mathbb{E}[\mathbf{X}]$	Covariance matrix $\mathbb{E}[(\mathbf{X} - \mathbb{E}[\mathbf{X}])(\mathbf{X} - \mathbb{E}[\mathbf{X}])^\intercal]$							
25 (mm)	6.25	3.7407	3.7407	3.1172	3.7407	3.7407	0	0
30 (mm)	3.7407	9.0000	4.4888	3.7407	4.4888	4.4888	0	0
30 (mm)	3.7407	4.4888	9.0000	3.7407	4.4888	4.4888	0	0
25 (mm)	3.1172	3.7407	3.7407	6.2500	3.7407	3.7407	0	0
30 (mm)	3.7407	4.4888	4.4888	3.7407	9.0000	4.4888	0	0
30 (mm)	3.7407	4.4888	4.4888	3.7407	4.4888	9.0000	0	0
203 (GPa)	0	0	0	0	0	0	103.02	0.0583
0.23	0	0	0	0	0	0	0.0583	0.0001

of the partitioned D-MORPH, using the same 350 FEA, produces practically the same results as the SLS regression. This is possible even if the number of FEA is larger than the number of coefficients, that is, when there is an overdetermined system. However, the true benefit of the partitioned D-MORPH is realized when nearly identical failure probabilities are obtained from only 50 and 150 FEA, yielding the corresponding underdetermined systems through the extended approach. Therefore, the partitioned D-MORPH regression enriches GPCE in providing not only an accurate estimation of the failure probability, but also in reducing the computational cost of the SLS regression by more than a factor of two.

8.4. Example 4: a piston-connecting rod-crankshaft assembly

The final example demonstrates the effectiveness of the proposed partitioned D-MORPH regression in solving a practical engineering problem. It involves a connecting rod, which connects a piston to a crankshaft in an internal combustion engine. Together with the crankshaft, the connecting rod forms a simple mechanism where a reciprocating motion of the piston is converted into a rotating motion, as shown in Fig. 4(a). Subsequently, the crankshaft transfers the motion to the wheels of an automobile through a flywheel, clutch assembly, and transmission and drive shaft systems. Due to harsh operating environments involving high temperature and pressure, engineers frequently perform stress analysis of the piston-connecting rod-crankshaft assembly to determine structural integrity. In this example, a stochastic stress analysis was performed by recognizing manufacturing variability in the tolerances of the connecting rod geometry and random elastic material properties. Fig. 4(b) depicts a computer-aided design (CAD) model of the connecting rod with six random manufacturing variables X_1 through X_6 marked in side and front views. Two remaining random variables X_7 and X_8 represent the Young's modulus and Poisson's ratio, respectively, of the material. Therefore, there are in total eight ($N = 8$) input random variables in this UQ problem. Table 5 describes the statistical properties of all eight input random variables. The manufacturing variables and material property variables are correlated among their own individual constituents, but there is no correlation between two individual groups of variables. The probability distribution of $\mathbf{X}$ is lognormal.

Fig. 5(a) describes the loading and boundary conditions of the piston-connecting rod-crankshaft assembly for a linear-elastic, quasi-static stress analysis. The piston head is inclined by 10 degrees with respect to the vertical axis of the connecting rod and is subjected to a constant pressure of 19 MPa. The piston is attached to the connecting rod with a rigid piston pin. Similarly, the connecting rod is joined with a rigid crankshaft, which is fixed in the global coordinate system. Given the CAD model, an FEA model of the assembly, encompassing 282,793 tetrahedral elements, was developed with the mesh at

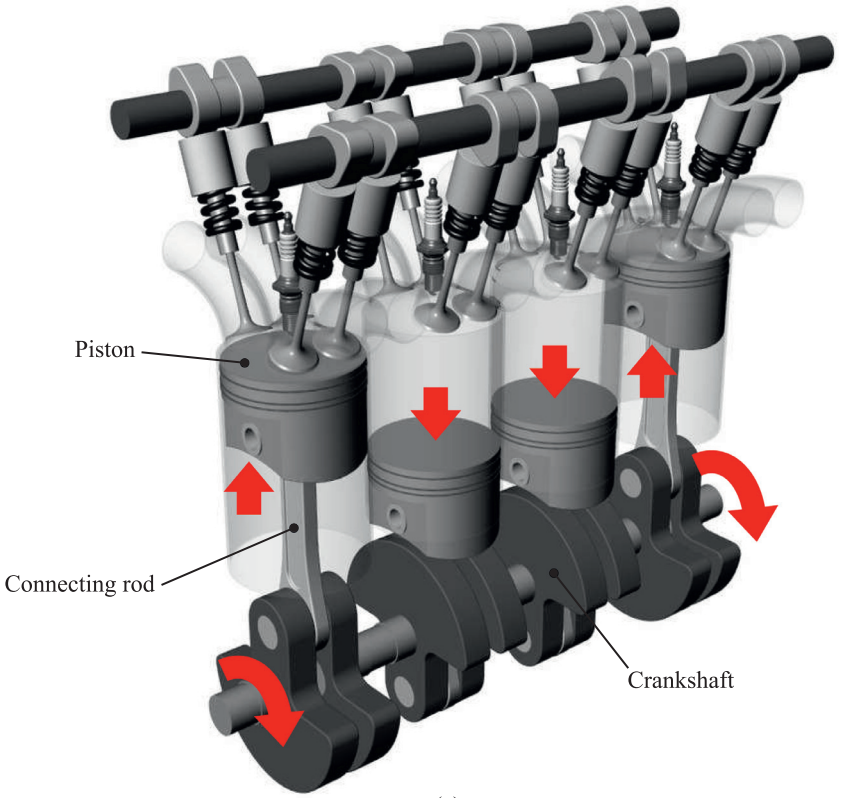

(a)

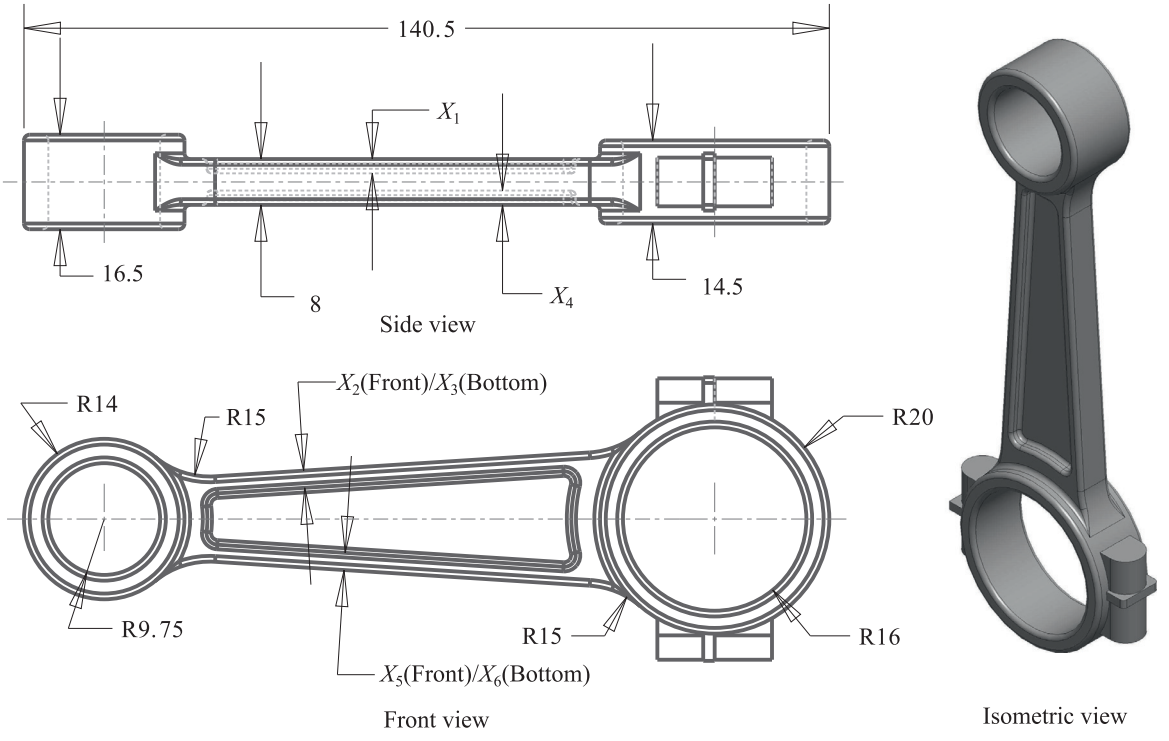

(b)

Fig. 4. An internal combustion engine (Example 4); (a) a stock photo of the piston-connecting rod-crankshaft assembly; (b) a CAD model of the connecting rod.

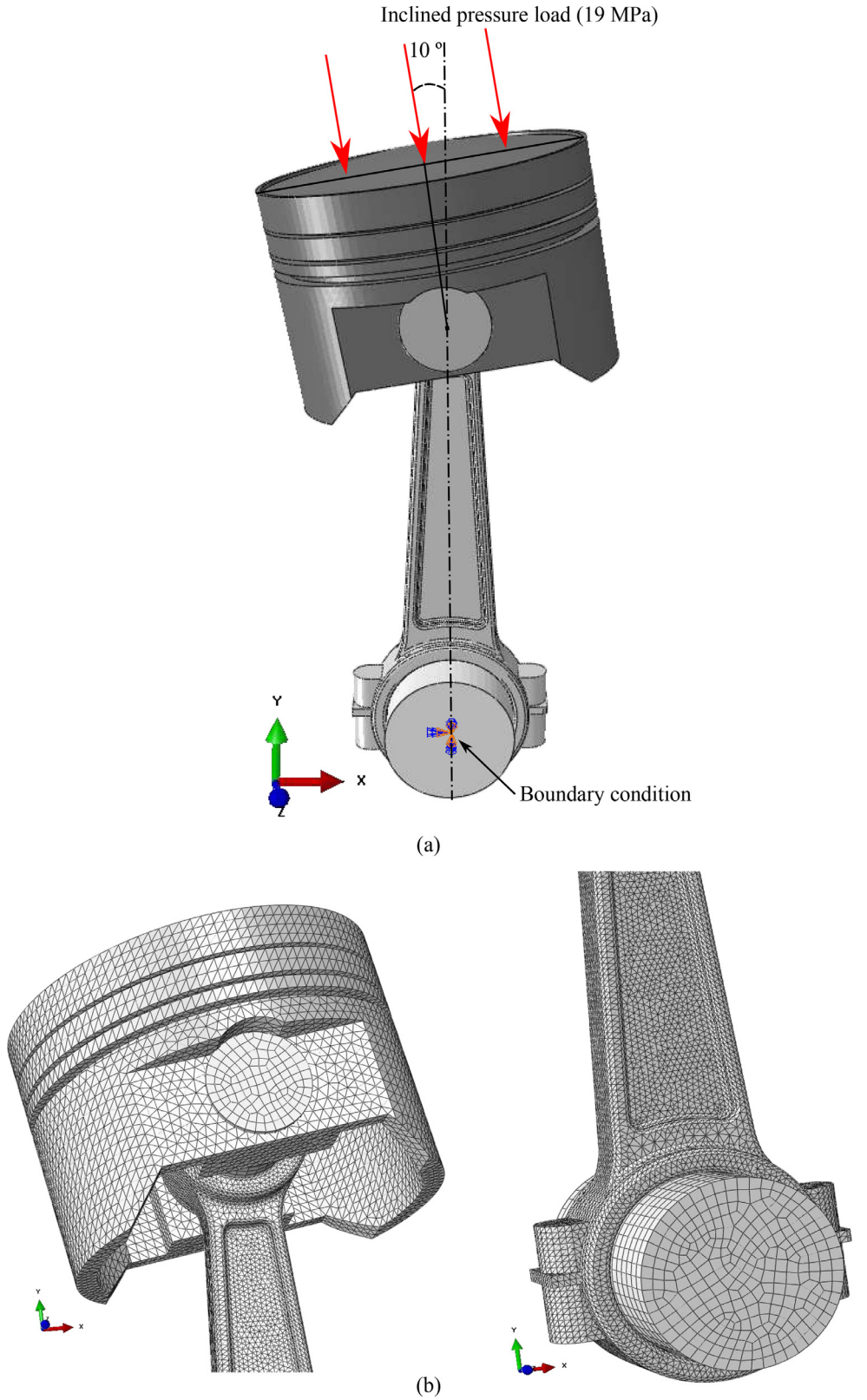

Fig. 5. An FEA of the piston-connecting rod-crankshaft assembly (Example 4); (a) loading and boundary conditions; (b) a tetrahedral mesh comprising 282,793 elements.

Table 6
Second-moment properties of two response measures by several GPCE approximations and standard MCS (Example 4).

Method	Max. von Mises stress (MPa)		Max. largest prin. strain (%)		Number of FEA
	Mean	Standard deviation	Mean	Standard deviation	
3rd order GPCE					
SLS	3691.62	156.40	0.7369	0.0507	1,650
Partitioned D-MORPH					
Extended approach[a]					
data size=100	3691.14	149.64	0.7435	0.0491	100
data size=250	3685.90	158.31	0.7364	0.0495	250
Direct approach[b]					
data size=350	3689.94	156.59	0.7360	0.0502	350
Standard MCS	3688.30	157.54	0.7365	0.0491	3,000

[a] $L_p = \lceil L/K_2 \rceil$, so extended approach is followed by direct approach according to Algorithm 1.
[b] $L_p = \lceil L_{N,m}/K_1 \rceil$, so only direct approach is used according to Algorithm 1.

mean input exhibited in Fig. 5(b). A CAD-FEA interface was developed in such a way that given a choice of the geometry parameters of CAD, the corresponding FEA mesh can be automatically generated. This facilitates a seamless calculation of the samples of a random output variable $y(\mathbf{X})$ for arbitrarily chosen samples of input random variables $\mathbf{X}$.

For the output variables, two response measures, frequently used in defining material failure criteria and fatigue durability analysis, were examined: von Mises stress and principal strain in the connecting rod. Fig. 6(a) and (b) portray the contour plots of the stress and strain when the input variables are fixed at their mean values. However, due to uncertain input $\mathbf{X}$, both response measures are random variables. The maximum value of the von Mises stress or the principal strain may not necessarily occur at a unique location of the connecting rod. Depending on the randomness of the geometry parameters, the location may vary from sample to sample, as shown in Fig. 6(c), for the maximum von Mises stress. This may lead to discontinuous responses[1], as observed in this example.

Table 6 summarizes the approximate means and standard deviations of the maximum von Mises stress and maximum principal strain calculated by a third-order GPCE approximation where the coefficients are estimated from both the SLS and partitioned D-MORPH regression analyses. Compared with the standard MCS-generated statistics (3000 samples), also listed in Table 6, all GPCE solutions reported provide very good to excellent estimates of the means and standard deviations of both responses at lower computational cost. However, to match the quality of the MCS result, the solution from the GPCE/SLS regression requires 1650 FEA, which is lower yet comparable to the cost of MCS. In other words, there is no significant cost reduction in the SLS regression. In contrast, the approximations from the GPCE/partitioned D-MORPH regression provide estimates of the second-moment properties as good as the MCS or GPCE/SLS regression, but costing only 100–350 FEA — an order of magnitude lower than that required by the two latter methods. As the number of basis or coefficients is $L_{8,3} = 165$, both underdetermined and overdetermined systems are encountered when performing the direct or, additionally, extended approaches of the partitioned D-MORPH regression according to Algorithm 1.

Fig. 7(a) and (b) display the approximate cumulative probability distribution functions (CDFs) of the maximum von Mises stress and maximum principal strain by a third-order GPCE approximation obtained in conjunction with the partitioned D-MORPH regression and 100–350 FEA. The distribution functions were obtained by resampling the GPCE approximation 10^6 times. The computational requirement of resampling, not to be confused with the standard MCS of an actual response, is negligible, as it involves evaluations of elementary polynomial functions describing the GPCE approximation. Due to the computational expense inherent in conducting FEA, the same 3000 realizations of output variables were employed to generate their respective distributions and are also plotted in Fig. 7(a) and (b). These MCS-generated distribution functions, given the low sample size, are not expected to describe accurate tail probabilistic characteristics. Nonetheless, the overall trends of the GPCE-produced distribution functions match the MCS results reasonably well. Again, the same computational expense from 100 to 350 FEA is incurred, demonstrating GPCE's ability in producing accurate probabilistic response characteristics as well.

Since the SLS or D-MORPH regression presented here entails Monte Carlo sampling, all input-output data sets were obtained objectively. Having said this, a more rigorous analysis should involve repeated samplings with different starting seeds to generate multiple such data sets and then developing statistics of the estimated moments and reliability. While the repeated samplings are unnecessary for the polynomial response functions in Example 2, they may be relevant to Examples 3 and 4, but at the expense of conducting significantly more FEA than what is reported. No statistical analysis was performed in this work for computational efficiency.

[1] For non-smooth stochastic output functions, an attractive alternative is to choose other types of basis functions, such as splines. In particular, a spline chaos expansion [27], comprising orthonormal B-splines, enables representation of locally prominent responses better than PCE equipped with orthonormal polynomials.

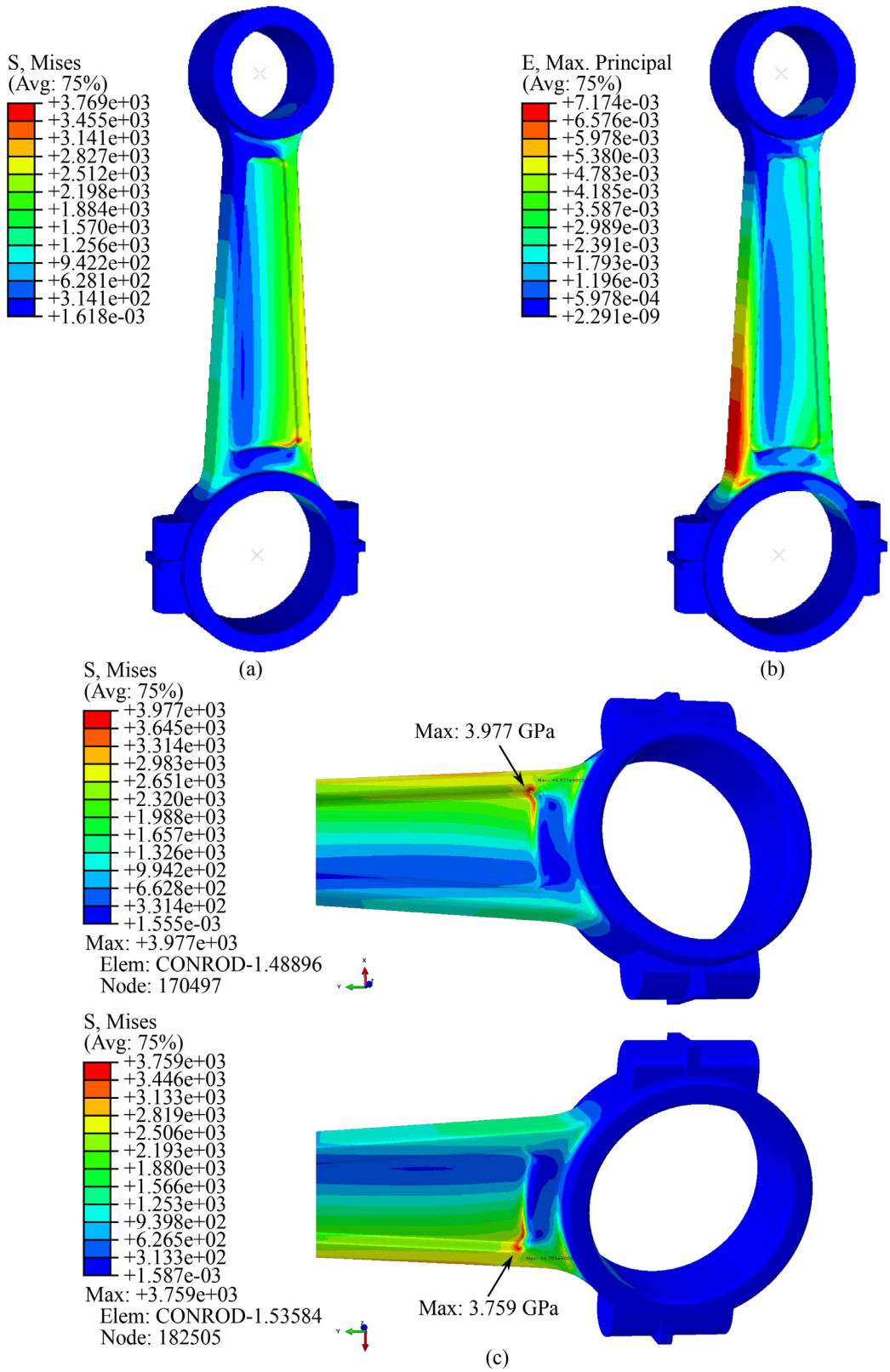

Fig. 6. Deterministic FEA results for the connecting rod (Example 4); (a) contours of von Mises stress at mean input; (b) contours of principal strain at mean input; (c) location shift of maximum von Mises stress from two samples of random input.

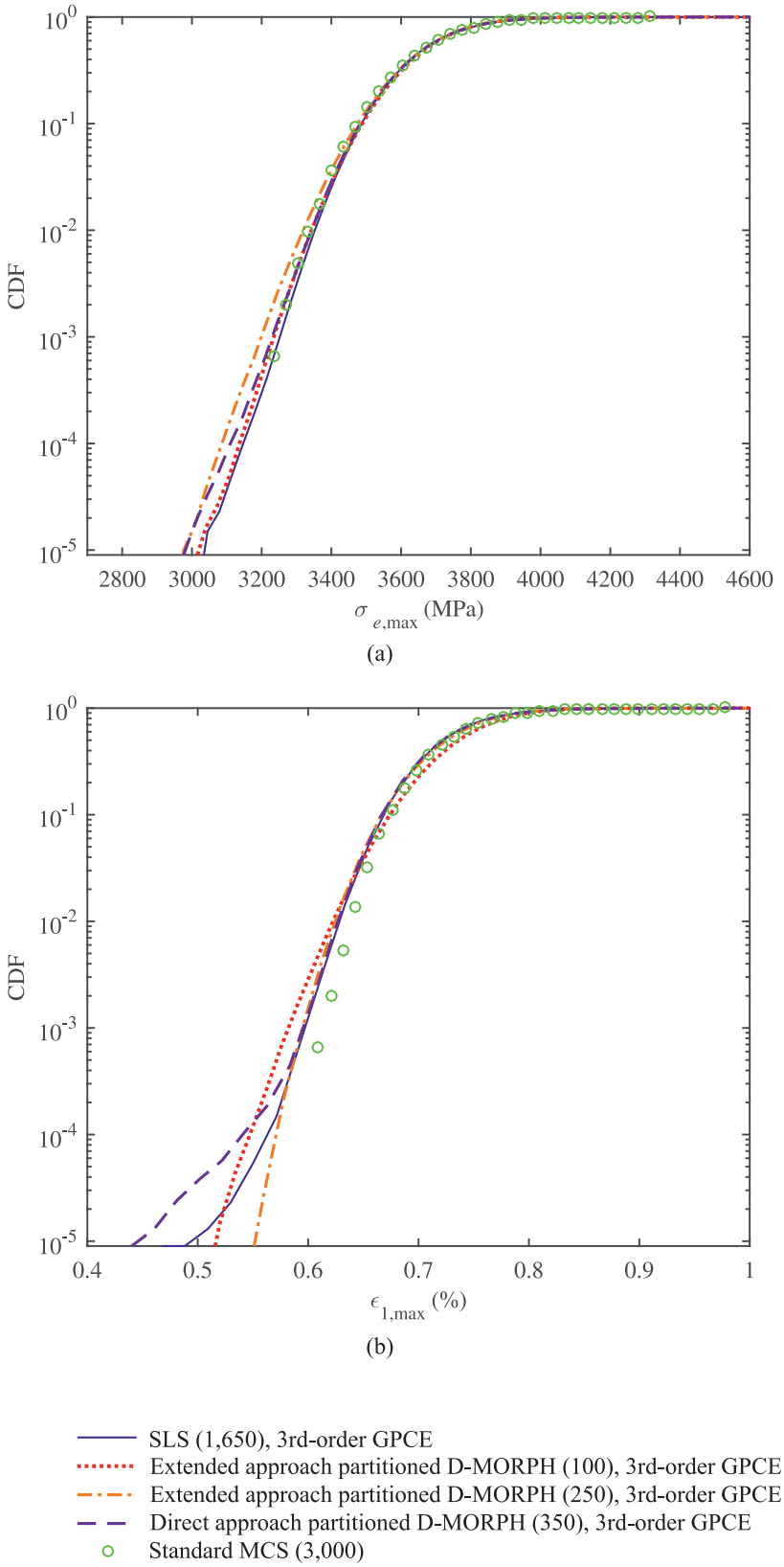

Fig. 7. Cumulative probability distribution functions of two responses in the connecting rod; (a) maximum von Mises stress $\sigma_{e,\max}$; (b) maximum largest principal strain $\epsilon_{1,\max}$ (Example 4).

9. Outlook

While the paper provides a practical approach for conducting UQ analysis under dependent variables, there are still a few open questions. The first one is identified with the exponential growth in the number of basis or expansion coefficients of GPCE. Indeed, from (15), $L_{N,m} = \mathcal{O}(N^m/m!)$ when $N \to \infty$. For UQ problems in stochastic dimensions higher than what is studied here, GPCE is not scalable, easily succumbing to the curse of dimensionality. Therefore, developments of alternative stochastic methods capable of exploiting low effective dimensions of high-dimensional functions, such as the GPDD method [13], are desirable. Unfortunately, existing GPDD is also not applicable for solving a general UQ problem under dependent variables. Obviously, constructing a practical version of GPDD is in order.

The second question is associated with a large number of Gauss integration points needed to estimate the monomial moment matrix $\mathbf{G}_m$. For instance, a 100-point Gauss quadrature rule was required in Case 3 of Example 1. Although no output function evaluations are involved, the computational effort of constructing $\mathbf{G}_m$ for high dimensional problems is still burdensome and should not be ignored. A multidimensional cubature rule, if it exists, for non-product-type probability measures is desired.

The third question is related to the development of an adaptive version of GPCE, where a truncated set of basis is selected optimally based on a specified error tolerated by the resulting approximation. By doing so, the need for arbitrarily deciding on the order of GPCE approximation is avoided. These questions are all subjects of current research in the authors' group.

10. Conclusion

A practical version of GPCE was created for computationally efficient UQ analysis in the presence of dependent input random variables, following a general, non-product-type probability distribution. The version has at least two important streams of novelties. First, a three-step computational algorithm, encompassing monomial basis, monomial moment matrix, and whitening transformation, was crafted to generate from scratch multivariate orthonormal polynomials that are consistent with the specified input probability distribution. Two numerical schemes, one derived from the Gauss quadrature and the other rooted in sampling approximations, were conceived to construct the monomial moment matrix. Unlike the Rodrigues-type formulae used in a prequel, the algorithm developed is capable of producing approximate orthonormal polynomials for a wide variety of input probability measures. Second, for UQ analysis under dependent random variables, two regression methods, comprising existing SLS and newly proposed partitioned D-MORPH, were exploited for the very first time to estimate GPCE's expansion coefficients economically. In contrast to the existing regression devoted so far to the classical PCE, no tensor-product structure is assumed or required. More importantly, the partitioned D-MORPH regression, which can be viewed as a modified variant of the original D-MORPH regression, is applicable to either an underdetermined or an overdetermined system, thereby markedly enhancing the power of the latter regression. The partitioned D-MORPH method should be useful not only in the context of GPCE as demonstrated here, but also in performing general high-dimensional regression analysis.

Numerical results obtained for Gaussian, Gegenbauer, and Dirichlet probability distributions demonstrate highly accurate sequences of measure-consistent multivariate orthonormal polynomials generated by the proposed three-step algorithm. However, care must be taken in defining the appropriate order of Gauss quadrature or the sample size when constructing the monomial moment matrix. This is chiefly because the condition number of the monomial moment matrix grows quickly with the order of the monomial basis. As long as the order is not overly large, as anticipated in a practical setting, measure-consistent orthonormal polynomials required by GPCE can be produced in a proficient manner.

Numerical results of UQ analysis, conducted for three mathematical functions and two solid-mechanics problems, indicate that the GPCE approximations, combined with SLS or partitioned D-MORPH regression for calculating the expansion coefficients, provide excellent estimates of the second-moment properties and reliability. Remarkably, the partitioned D-MORPH regression requires only a few hundreds of function evaluations or FEA compared with thousands of function evaluations of FEA mandated by the SLS regression. Therefore, a GPCE approximation, in conjunction with the partitioned D-MORPH regression, delivers a hefty computational advantage for UQ analysis under dependent random variables.

Appendix A. Results of Example 1

Tables A.1–A.3 provide orthonormal polynomials for Example 1.

Table A.1
Exact orthonormal polynomials for Gaussian, Gegenbauer, and Dirichlet density functions (Example 1).

Case 1: Gaussian density on $\mathbb{R}^2$ ($\sigma_1 = \sigma_2 = 1/4, \rho = 2/5$)

$\Psi_1(x_1, x_2) = 1,$

$\Psi_2(x_1, x_2) = 4x_1,$

$\Psi_3(x_1, x_2) \approx -1.74574x_1 + 4.36436x_2,$

$\Psi_4(x_1, x_2) \approx 11.31371x_1^2 - 0.70711,$

$\Psi_5(x_1, x_2) \approx -6.98297x_1^2 + 17.45743x_1x_2,$

$\Psi_6(x_1, x_2) \approx 2.15499x_1^2 - 10.77496x_2x_1 + 13.46870x_2^2 - 0.70711,$

$\Psi_7(x_1, x_2) \approx 26.12789x_1^3 - 4.89898x_1,$

$\Psi_8(x_1, x_2) \approx -19.75083x_1^3 + 49.37707x_2x_1^2 + 1.23443x_1 - 3.08607x_2,$

$\Psi_9(x_1, x_2) \approx 8.61997x_1^3 - 43.09984x_2x_1^2 + 53.87480x_2^2x_1 - 2.82843x_1,$

$\Psi_{10}(x_1, x_2) \approx -2.17203x_1^3 + 16.290209x_2x_1^2 - 40.72552x_2^2x_1 + 2.13809x_1 + 33.93794x_2^3 - 5.34522x_2.$

Case 2: Density on the disk $\mathbb{B}^2$ ($\mu = 4$)

$\Psi_1(x_1, x_2) = 1,$

$\Psi_2(x_1, x_2) \approx 3.31662x_1,$

$\Psi_3(x_1, x_2) \approx 3.31662x_2,$

$\Psi_4(x_1, x_2) \approx 8.86848x_1^2 - 0.80623,$

$\Psi_5(x_1, x_2) \approx 11.95826x_1x_2,$

$\Psi_6(x_1, x_2) \approx 0.89132x_1^2 + 8.91316x_2^2 - 0.89132,$

$\Psi_7(x_1, x_2) \approx 21.55806x_1^3 - 4.97494x_1,$

$\Psi_8(x_1, x_2) \approx 34.08629x_1^2x_2 - 2.62202x_2,$

$\Psi_9(x_1, x_2) \approx 3.45205x_1^3 + 34.52053x_2^2x_1 - 3.45205x_1,$

$\Psi_{10}(x_1, x_2) \approx 21.83270x_2^3 + 5.45817x_1^2x_2 - 5.45817x_2.$

Case 3: Density on the triangle $\mathbb{T}^2$ ($\alpha = \beta = \gamma = 3$)

$\Psi_1(x_1, x_2) = 1,$

$\Psi_2(x_1, x_2) \approx 7.64853x_1 - 2.54951,$

$\Psi_3(x_1, x_2) \approx 4.41588x_1 + 8.83176x_2 - 4.41588,$

$\Psi_4(x_1, x_2) \approx 45.50000x_1^2 - 32.50000x_1 + 5.00000,$

$\Psi_5(x_1, x_2) \approx 37.85829x_1^2 + 75.71658x_2x_1 - 48.67494x_1 - 21.63331x_2 + 10.81665,$

$\Psi_6(x_1, x_2) \approx 13.49074x_1^2 + 60.70832x_2x_1 - 26.98148x_1 + 60.70832x_2^2 - 60.70832x_2 + 13.49074,$

$\Psi_7(x_1, x_2) \approx 240.32201x_1^3 - 270.36226x_1^2 + 90.12075x_1 - 8.58293,$

$\Psi_8(x_1, x_2) \approx 246.48511x_1^3 + 492.97022x_2x_1^2 - 400.53830x_1^2 - 308.10639x_2x_1 + 174.59362x_1 + 41.08085x_2 - 20.54043,$

$\Psi_9(x_1, x_2) \approx 128.45752x_1^3 + 578.05882x_2x_1^2 - 289.02941x_1^2 + 578.05882x_2^2x_1 - 722.57353x_2x_1 + 192.68627x_1 - 144.51471x_2^2 + 144.51471x_2 - 32.11438,$

$\Psi_{10}(x_1, x_2) \approx 33.54238x_1^3 + 251.56781x_2x_1^2 - 100.62712x_1^2 + 553.44918x_2^2x_1 - 503.13562x_2x_1 + 100.62712x_1 + 368.96612x_2^3 - 553.44918x_2^2 + 251.56781x_2 - 33.54238.$

Table A.2
Approximate orthonormal polynomials for Gaussian, Gegenbauer, and Dirichlet density functions obtained when the monomial moment matrix is constructed by numerical integration (Example 1).

Case 1: Gaussian density on $\mathbb{R}^2$ ($\sigma_1 = \sigma_2 = 1/4, \rho = 2/5$)

$\tilde{\Psi}_1(x_1, x_2) = 1,$

$\tilde{\Psi}_2(x_1, x_2) \approx 4.00000x_1,$

$\tilde{\Psi}_3(x_1, x_2) \approx -1.74574x_1 + 4.36436x_2,$

$\tilde{\Psi}_4(x_1, x_2) \approx 11.31371x_1^2 - 0.70711,$

$\tilde{\Psi}_5(x_1, x_2) \approx -6.98297x_1^2 + 17.45743x_2x_1,$

$\tilde{\Psi}_6(x_1, x_2) \approx 2.15499x_1^2 - 10.77496x_2x_1 + 13.46870x_2^2 - 0.70711,$

$\tilde{\Psi}_7(x_1, x_2) \approx 26.12789x_1^3 - 4.89898x_1,$

$\tilde{\Psi}_8(x_1, x_2) \approx -19.75080x_1^3 + 49.37707x_2x_1^2 + 1.23443x_1 - 3.08607x_2,$

$\tilde{\Psi}_9(x_1, x_2) \approx 8.61997x_1^3 - 43.09984x_2x_1^2 + 53.87480x_2^2x_1 - 2.82843x_1,$

$\tilde{\Psi}_{10}(x_1, x_2) \approx -2.17203x_1^3 + 16.29021x_2x_1^2 - 40.72552x_2^2x_1 + 2.13809x_1 + 33.93794x_2^3 - 5.34522x_2.$

(*continued on next page*)

Table A.2 (*continued*)

Case 2: Density on the disk $\mathbb{B}^2$ ($\mu = 4$)

$\tilde{\Psi}_1(x_1, x_2) = 1$,
$\tilde{\Psi}_2(x_1, x_2) \approx 3.31713x_1$,
$\tilde{\Psi}_3(x_1, x_2) \approx 3.31713x_2$,
$\tilde{\Psi}_4(x_1, x_2) \approx 8.87909x_1^2 - 0.80694$,
$\tilde{\Psi}_5(x_1, x_2) \approx 11.96837x_1x_2$,
$\tilde{\Psi}_6(x_1, x_2) \approx 0.89932x_1^2 + 8.92452x_2^2 - 0.89280$,
$\tilde{\Psi}_7(x_1, x_2) \approx 21.67098x_1^3 - 4.99408x_1$,
$\tilde{\Psi}_8(x_1, x_2) \approx 34.20159x_2x_1^2 - 2.62726x_2$,
$\tilde{\Psi}_9(x_1, x_2) \approx 3.54251x_1^3 + 34.65554x_2^2x_1 - 3.47850x_1$,
$\tilde{\Psi}_{10}(x_1, x_2) \approx 21.95861x_2^3 + 5.59086x_1^2x_2 - 5.48984x_2$.

Case 3: Density on the triangle $\mathbb{T}^2$ ($\alpha = \beta = \gamma = 3$)

$\tilde{\Psi}_1(x_1, x_2) = 1$,
$\tilde{\Psi}_2(x_1, x_2) \approx 7.64883x_1 - 2.5496$,
$\tilde{\Psi}_3(x_1, x_2) \approx 4.41575x_1 + 8.83195x_2 - 4.41589$,
$\tilde{\Psi}_4(x_1, x_2) \approx 45.52738x_1^2 - 32.51715x_1 + 0.00053x_2 + 5.00209$,
$\tilde{\Psi}_5(x_1, x_2) \approx 37.85422x_1^2 + 75.72173x_2x_1 - 48.67316x_1 - 21.63521x_2 + 10.81666$,
$\tilde{\Psi}_6(x_1, x_2) \approx 13.46087x_1^2 + 60.64759x_2x_1 - 26.94144x_1 + 60.71700x_2^2 - 60.69386x_2 + 13.48155$,
$\tilde{\Psi}_7(x_1, x_2) \approx 241.33885x_1^3 - 271.36060x_1^2 + 0.01244x_2x_1 + 90.40171x_1 - 0.00657x_2^2 + 0.00023x_2 - 8.60480$,
$\tilde{\Psi}_8(x_1, x_2) \approx 246.42502x_1^3 + 493.08016x_2x_1^2 - 400.47291x_1^2 - 308.09092x_2x_1 + 174.54661x_1 + 0.10572x_2^2 + 40.99122x_2 - 20.51907$,
$\tilde{\Psi}_9(x_1, x_2) \approx 127.52486x_1^3 + 576.13301x_2x_1^2 - 287.42400x_1^2 + 578.17692x_2^2x_1 - 721.28150x_2x_1 + 191.92253x_1 - 144.54735x_2^2 + 144.32192x_2 - 32.01224$,
$\tilde{\Psi}_{10}(x_1, x_2) \approx 32.18986x_1^3 + 247.65922x_2x_1^2 - 98.03983x_1^2 + 549.47369x_2^2x_1 - 498.04315x_2x_1 + 99.02324x_1 + 368.91175x_2^3 - 552.22235x_2^2 + 250.39142x_2 - 33.26058$.

Table A.3
Approximate orthonormal polynomials for Gaussian, Gegenbauer, and Dirichlet density functions obtained when the monomial moment matrix is constructed by QMCS (Example 1).

Case 1: Gaussian density on $\mathbb{R}^2$ ($\sigma_1 = \sigma_2 = 1/4$, $\rho = 2/5$)

$\tilde{\Psi}_1(x_1, x_2) = 1$,
$\tilde{\Psi}_2(x_1, x_2) \approx 3.99998x_1$,
$\tilde{\Psi}_3(x_1, x_2) \approx -1.74338x_1 + 4.36625x_2 + 0.00016$,
$\tilde{\Psi}_4(x_1, x_2) \approx 11.31273x_1^2 - 0.00035x_1 + 0.00052x_2 - 0.70705$,
$\tilde{\Psi}_5(x_1, x_2) \approx -6.95962x_1^2 + 17.45190x_2x_1 + 0.00154x_1 - 0.00056x_2 - 0.00054$,
$\tilde{\Psi}_6(x_1, x_2) \approx 2.13768x_1^2 - 10.76093x_2x_1 + 0.00068x_1 + 13.48920x_2^2 - 0.00262x_2 - 0.70704$,
$\tilde{\Psi}_7(x_1, x_2) \approx 26.11043x_1^3 + 0.00386x_1^2 - 0.01745x_2x_1 - 4.89703x_1 - 0.00154x_2^2 + 0.00193x_2 + 0.00027$,
$\tilde{\Psi}_8(x_1, x_2) \approx -19.49070x_1^3 + 49.22380x_2x_1^2 - 0.00384x_1^2 - 0.03253x_2x_1 + 1.20261x_1 + 0.02985x_2^2 - 3.08110x_2 - 0.00069$,
$\tilde{\Psi}_9(x_1, x_2) \approx 8.51366x_1^3 - 43.06678x_2x_1^2 - 0.02133x_1^2 + 53.86837x_2^2x_1 + 0.04443x_2x_1 - 2.81454x_1 - 0.00015x_2^2 + 0.00585x_2 + 0.00014$,
$\tilde{\Psi}_{10}(x_1, x_2) \approx -2.14148x_1^3 + 16.11466x_2x_1^2 + 0.00859x_1^2 - 40.73595x_2^2x_1 + 0.02361x_2x_1 + 2.13951x_1 + 34.16904x_2^3 - 0.02837x_2^2 - 5.36768x_2 + 0.00016$.

Case 2: Density on the disk $\mathbb{B}^2$ ($\mu = 4$)

$\tilde{\Psi}_1(x_1, x_2) = 1$,
$\tilde{\Psi}_2(x_1, x_2) \approx 3.32066x_1 - 0.00061$,
$\tilde{\Psi}_3(x_1, x_2) \approx -0.00154x_1 + 3.31969x_2 + 0.00046$,
$\tilde{\Psi}_4(x_1, x_2) \approx 8.89912x_1^2 + 0.00077x_1 - 0.00097x_2 - 0.80705$,
$\tilde{\Psi}_5(x_1, x_2) \approx -0.01119x_1^2 + 12.00233x_2x_1 + 0.00036x_1 - 0.00125x_2 + 0.00051$,
$\tilde{\Psi}_6(x_1, x_2) \approx 0.91148x_1^2 - 0.00933x_2x_1 + 0.00078x_1 + 8.93982x_2^2 + 0.00088x_2 - 0.89387$,
$\tilde{\Psi}_7(x_1, x_2) \approx 21.76503x_1^3 + 0.00555x_1^2 + 0.01301x_2x_1 - 5.00433x_1 + 0.00219x_2^2 - 0.00142x_2 + 0.00002$,
$\tilde{\Psi}_8(x_1, x_2) \approx -0.03882x_1^3 + 34.34533x_2x_1^2 + 0.01253x_1^2 + 0.01237x_2x_1 + 0.00424x_1 - 0.01781x_2^2 - 2.62744x_2 + 0.00021$,
$\tilde{\Psi}_9(x_1, x_2) \approx 3.58612x_1^3 - 0.07155x_2x_1^2 + 0.00649x_1^2 + 34.83983x_2^2x_1 - 0.02912x_2x_1 - 3.49135x_1 - 0.00027x_2^2 + 0.00269x_2 - 0.00029$,
$\tilde{\Psi}_{10}(x_1, x_2) \approx -0.00663x_1^3 + 5.70671x_2x_1^2 - 0.00719x_1^2 - 0.04585x_2^2x_1 + 0.00657x_2x_1 + 0.00421x_1 + 22.03289x_2^3 + 0.00531x_2^2 - 5.50588x_2 - 0.00008$.

(*continued on next page*)

Table A.3 (*continued*)

Case 3: Density on the triangle $\mathbb{T}^2$ ($\alpha = \beta = \gamma = 3$)

$\tilde{\Psi}_1(x_1, x_2) = 1,$

$\tilde{\Psi}_2(x_1, x_2) \approx 7.64850x_1 - 2.54950,$

$\tilde{\Psi}_3(x_1, x_2) \approx 4.42211x_1 + 8.83491x_2 - 4.41896,$

$\tilde{\Psi}_4(x_1, x_2) \approx 45.49801x_1^2 - 32.49920x_1 - 0.00088x_2 + 5.00028,$

$\tilde{\Psi}_5(x_1, x_2) \approx 37.91010x_1^2 + 75.71620x_2x_1 - 48.70801x_1 - 21.63168x_2 + 10.82123,$

$\tilde{\Psi}_6(x_1, x_2) \approx 13.50575x_1^2 + 60.77797x_2x_1 - 27.01228x_1 + 60.73453x_2^2 - 60.75559x_2 + 13.50575,$

$\tilde{\Psi}_7(x_1, x_2) \approx 240.25275x_1^3 - 270.34377x_1^2 - 0.08134x_2x_1 + 90.16094x_1 + 0.02853x_2^2 + 0.00489x_2 - 8.59185,$

$\tilde{\Psi}_8(x_1, x_2) \approx 246.55338x_1^3 + 492.81872x_2x_1^2 - 400.58113x_1^2 - 307.90457x_2x_1 + 174.57489x_1 + 0.08602x_2^2 + 40.97078x_2 - 20.52165,$

$\tilde{\Psi}_9(x_1, x_2) \approx 128.23251x_1^3 + 577.67455x_2x_1^2 - 288.61332x_1^2 + 577.63701x_2^2x_1 - 721.92156x_2x_1 + 192.41323x_1 - 144.37246x_2^2 + 144.34645x_2 - 32.06350,$

$\tilde{\Psi}_{10}(x_1, x_2) \approx 32.49494x_1^3 + 249.80446x_2x_1^2 - 98.96153x_1^2 + 552.52149x_2^2x_1 - 501.46783x_2x_1 + 99.83755x_1 + 369.12190x_2^3 - 553.42161x_2^2 + 251.35466x_2 - 33.44923.$

References

[1] N. Wiener, The homogeneous chaos, Am. J. Math. 60 (4) (1938) 897–936.
[2] R.H. Cameron, W.T. Martin, The orthogonal development of non-linear functionals in series of fourier-Hermite functionals, Ann. Math. 48 (1947) 385–392.
[3] S. Rahman, A polynomial dimensional decomposition for stochastic computing, Int J Numer Methods Eng 76 (2008) 2091–2116.
[4] S. Rahman, Mathematical properties of polynomial dimensional decomposition, SIAM/ASA J. Uncertain. Quant. 6 (2018) 816–844.
[5] I. Babuska, F. Nobile, R. Tempone, A stochastic collocation method for elliptic partial differential equations with random input data, SIAM J. Numer. Anal. 45 (3) (2007) 1005–1034.
[6] B. Ganapathysubramanian, N. Zabaras, Sparse grid collocation schemes for stochastic natural convection problems, J. Comput. Phys. 225 (1) (2007) 652–685.
[7] S. Smolyak, Quadrature and interpolation formulas for tensor products of certain classes of functions, Dokl. Akad. Nauk SSSR 4 (1963) 240–243.
[8] T. Gerstner, M. Griebel, Numerical integration using sparse grids, Numer. Algorithms 18 (1998) 209–232.
[9] Y. Noh, K.K. Choi, L. Du, Reliability-based design optimization of problems with correlated input variables using a gaussian copula, Struct. Multidiscip. Optim. 38 (2009) 1–16.
[10] M. Rosenblatt, Remarks on a multivariate transformation, Ann. Math. Stat. 23 (1952) 470–472.
[11] S. Rahman, Extended polynomial dimensional decomposition for arbitrary probability distributions, J. Eng. Mech. 135 (12) (2009) 1439–1451.
[12] S. Rahman, A polynomial chaos expansion in dependent random variables, J. Math. Anal. Appl. 464 (2018) 749–775.
[13] S. Rahman, Uncertainty quantification under dependent random variables by a generalized polynomial dimensional decomposition, Comput. Methods Appl. Mech. Eng. 344 (2019a) 910–937.
[14] S. Rahman, Dimension-wise multivariate orthogonal polynomials in general probability spaces, Appl. Math. Comput. 362 (2019b) 1–19.
[15] C.F. Dunkl, Y. Xu, Orthogonal Polynomials of Several Variables, Encyclopedia of mathematics and its applications 155, 2nd, Cambridge University Press, 2001.
[16] M. Navarro, J. Witteveen, J. Blom, Polynomial chaos expansion for general multivariate distributions with correlated variables (2014) 1–24. arXiv: 1406.5483.
[17] A. Kessy, A. Lewin, K. Strimmer, Optimal whitening and decorrelation, Am. Stat. 72 (4) (2018) 309–314.
[18] W. Gautschi, Orthogonal Polynomials: Computation and Approximation, Numerical mathematics and scientific computation, Oxford University Press, 2004.
[19] W.J. Morokoff, R.E. Caflisch, Quasi-monte carlo integration, J. Comput. Phys. 122 (1995) 218–230.
[20] I.M. Sobol, Distribution of points in a cube and approximate evaluation of integrals, Zh. Vych. Mat. Mat. Fiz. 7 (1967) 784–802.
[21] J.M. Taylor, The condition of gram matrices and related problems, Proc. R. Soc. Edinburgh 80A (1978) 45–56.
[22] A. Owen, Detecting Near Linearity in High Dimensions, Technical Report, Stanford University, Department of Statistics, 1998.
[23] G. Li, H. Rabitz, D-MORPH Regression: application to modeling with unknown parameters more than observation data, J. Math. Chem. 48 (2010) 1010–1035.
[24] G. Blatman, Adaptive Sparse Polynomial Chaos Expansions for Uncertainty Propagation and Sensitivity Analysis, Universite Blaise Pascal, Clermont-Ferrand, France, 2009 Ph.D. thesis.
[25] R. Penrose, A generalized inverse for matrices, Math. Proc. Cambridge Philos. Soc. 51 (1955) 406–413.
[26] G. Li, H. Rabitz, D-MORPH Regression for modeling with fewer unknown parameters than observation data, J Math Chem 50 (2012) 1747–1764.
[27] S. Rahman, A spline chaos expansion, SIAM/ASA J. Uncertain. Quant. 8 (2020) 27–57.